Accepted Manuscript

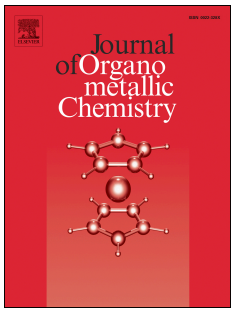

New phosphorus ylide palladacyclic: Synthesis, characterization, X-Ray crystal structure, biomolecular interaction studies, molecular docking and in vitro cytotoxicity evaluations

Kazem Karami, Mahzad Rahimi, Mostafa Zakariazadeh, Orhan Buyukgungor, Zahra Amirghofran

PII: S0022-328X(18)30542-4

DOI: 10.1016/j.jorganchem.2018.09.018

Reference: JOM 20575

To appear in: *Journal of Organometallic Chemistry*

Received Date: 1 July 2018

Revised Date: 12 September 2018

Accepted Date: 21 September 2018

Please cite this article as: K. Karami, M. Rahimi, M. Zakariazadeh, O. Buyukgungor, Z. Amirghofran, New phosphorus ylide palladacyclic: Synthesis, characterization, X-Ray crystal structure, biomolecular interaction studies, molecular docking and in vitro cytotoxicity evaluations, *Journal of Organometallic Chemistry* (2018), doi: https://doi.org/10.1016/j.jorganchem.2018.09.018.

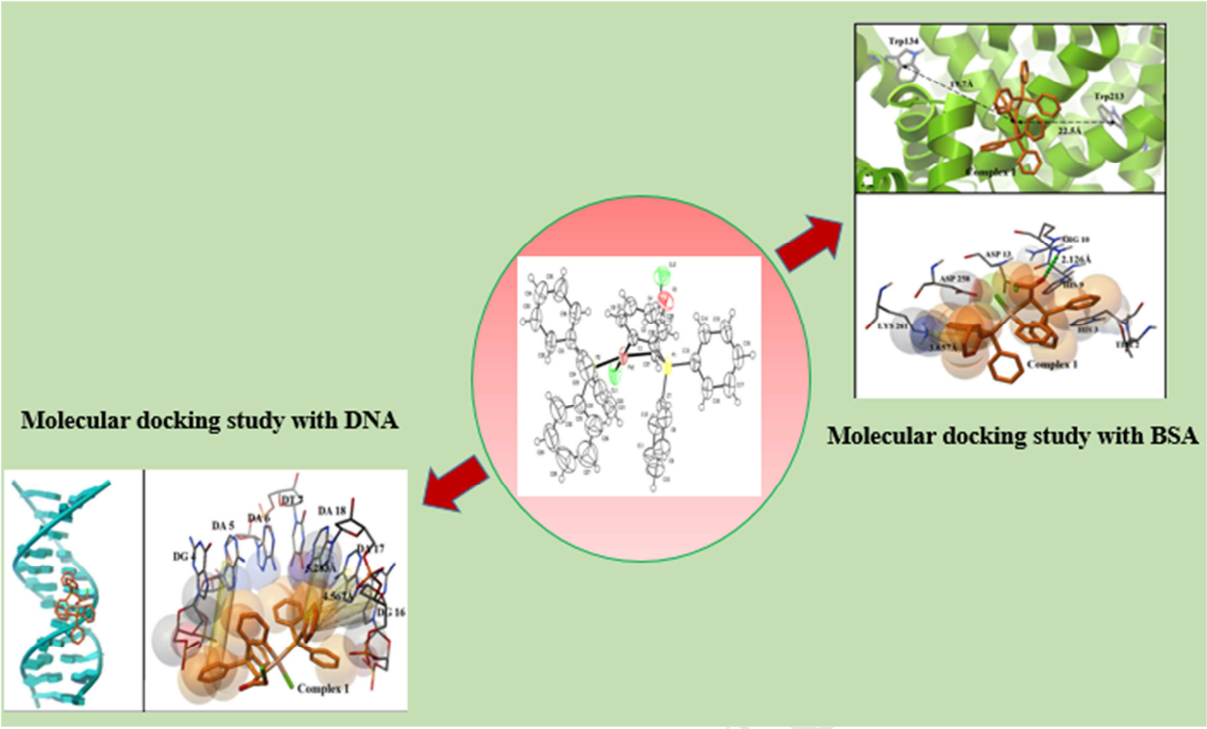

New phosphorus ylide palladacyclic: Synthesis, characterization, X-Ray crystal structure, biomolecular interaction studies, molecular docking and in vitro cytotoxicity evaluations

Kazem Karami[a*], Mahzad Rahimi[a], Mostafa Zakariazadeh[b], Orhan Buyukgungor[c], Zahra Amirghofran[d]

[a]Department of Chemistry, Isfahan University of Technology, Isfahan, 84156/83111, I.R. Iran
[b]Research Institute for Fundamental Sciences (RIFS), University of Tabriz, Tabriz, Iran
[c]Faculty of Arts and Sciences, Department of Physics , Ondokuz, Mayıs University, 55139 Samsun
d Immunology Department, Autoimmune Diseases Research center, Shiraz University of Medical Sciences, Shiraz 71454, Iran

Abstract

The ylide-phosphonium salt $[PPh_3CH_2C(O)CH_2Cl]^+Cl^-$ was reacted with $Pd(OAc)_2$ to give the chloro-bridged dinuclear complex $[Pd\{C(H)PPh_3C(O)CH_2Cl\}(\mu\text{-}Cl)(OAc)]_2$, which experienced bridge cleavage reactions with triphenylphosphine (PPh_3) and pyridine (Py), and to prepare the new orthometallated complexes $[Pd\{(C,C)\text{-}C_6H_4PPh_2C(H)C(O)CH_2Cl\}L]Cl$, [L=$PPh_3$ (**1**) and Py (**2**)]. The complexes were identified and characterized using various techniques. X-ray crystallography was used to determine the crystal structure of **1,** which revealed the presence of an orthometallated C_6H_4-PPh_2 unit. CT-DNA binding interaction of the synthesis compounds was tested by fluorescence spectroscopy, UV-Vis absorption spectroscopy, and the viscometric titration method. The analysis of the obtained data indicated that the Pd complexes could bind to DNA via groove binding by the partial intercalation mode. The emission titration of bovine serum albumin (BSA) with two Pd complexes showed a static process for the fluorescence quenching mechanism of BSA. In addition, the results of competitive binding by Eosin-Y, Ibuprofen and Digoxin site markers revealed that the complexes were bound to the site I of BSA. The donor (BSA) - acceptor (Pd complexes) distance was calculated using fluorescence resonance energy transfer (FRET). Notably, molecular docking studies were used for the determination of DNA and BSA-Pd (II) complexes binding. Finally, the two complexes exhibited significant *in vitro* cytotoxicity

against human leukemic T cell (Jurkat) and chronic myelogenous leukemia (K562) cancer cell lines using MTT([3-(4,5-dimethylthiazol-2-yl)-2,5-diphenyl-tetrazolium bromide] colorimetric. In cell cycle analysis conducted on Jurkat and K562 cells treated with ligand and Pd complexes, a decrease in DNA cell content and shift in the main population of cells toward the subG1 phase were observed.

Keyword: Orthometallated complexes; BSA binding; CT-DNA binding; Anticancer activity; Molecular docking

1. Introduction

Phosphorus ylides are useful ligands in many synthesis due to their ambidentate characters [1,2]. The reactivity and coordination chemistry of them are important in organometallic chemistry and their application in synthetic chemistry has been well recorded [3,4]. Recently, orthometallation of these ligands has been reported by many researchers because of regioselectivity at Ph rings of the phosphine, showing that the orthopalladated complexes derived from CH activation at Ph rings belong to the R′ or R″ substituents of the ylidic carbon [5,6]. Because of some problems associated with platinum-based anticancer drugs, such as limited solubility, limited spectrum of tumors, ototoxicity and neurotoxicity, significant attempts are being made to improve the effectiveness of them [7]. Thus, various new complexes have been synthesized in order to overcome those disadvantages. The complexes of ylide palladacyclic have received special attention due to their potential application in organic synthesis [5]. Ylide palladacyclic is a heterogeneous cyclic organic compound; palladium is the core of a specific structure stabilized by intramolecular connections [8]. Recently, the preparation of a wide variety of new complexes with medicinal properties such as anticancer activity and their biomolecular interaction studies has been reported [9,10].

Among metal-based complexes, palladium complexes are interesting anticancer drugs [11,12]. Anticancer properties of ylide palladacyclic have been specified due to their cytotoxity assessment [13]. The initial way for cancer therapy will be metallodrugs started in the interaction between DNA and coordination complexes [14]. There are three important styles of interactions between DNA and metal complexes; these include intercalation, groove binding and electrostatic interaction [15].

The most abundant proteins in blood plasma are serum albumins, whose major physiological function is to carry various ligands to a particular target organ [16]. Bovine Serum Albumin (BSA) was chosen because of the advantages of low price and accessibility and the similarity of the tertiary structure to the human serum albumin (HSA). Moreover, three sites of albumins are the specific binding sites for pharmaceutical metals [17-19].

In our work, synthesis of two new phosphorus ylide palladacyclic complexes was done using triphenylphosphine (PPh_3) and pyridine (Py) , something not reported before; then it was characterized by Elemental analysis, spectroscopic methods (UV-vis, FT-IR and NMR), and single crystal X-ray structure analysis. Additionally, biological application of them has been reported. Because of medical significance, low charge, easy accessibility, natural fluorescence emission, and the structural similarity of bovine serum albumin (BSA) with human serum albumin (HSA), it was utilized as the protein modeling for drug delivery [20,21]. The BSA binding capacity and site selective binding were monitored by UV absorption and fluorescence spectroscopy in the absence and presence of the complexes. In addition, the complex-DNA interaction was verified by UV visible absorption and fluorescence emission spectroscopy, molecular docking, and the viscometery method. Furthermore, the molecular docking technique was performed on BSA. Additionally, the prepared complexes exhibited antitumor activity and cytotoxic activity against human leukemic T cell (Jurkat) and chronic myelogenous leukemia (K562) cancer cell lines, as

evaluated by the MTT ([3-(4,5-dimethylthiazol-2-yl)-2,5-diphenyl-tetrazolium bromide]assay.

2. Experimental

2.1. Materials

All solvents and starting materials were obtained from Sigma Aldrich or Alfa Aesar and used without further purification. Methylene blue (MB), Calf thymus DNA (CT-DNA), and BSA were supplied by Sigma Aldrich. Stock solutions of BSA and CT-DNA were prepared by dissolving in a Tris buffer (NaCl (50 mM), Tris–HCl (5 mM) at the pH of 7.3). The UV absorbance ratio (A_{260}/A_{280}) of the solutions of CT-DNA was over 1.8, showing the purity of DNA [22]. The CT-DNA concentration was standardized by the UV-Vis absorption method, using its molar absorption coefficient (ε = 6600 M^{-1} cm^{-1}) [23,24]. Distilled deionized water as the solvent and dimethylsulfoxide (DMSO) as the co-solvent were used for the preparation of the stock solution of the complex. The final DMSO concentration never exceeded 0.13% (v/v). Jurkat (human leukemic T cell line) chronic myelogenous leukemia (K562) was bought from the National Cell Bank of Pasteur Institute, Tehran, Iran.

2.2. Measurements

Infrared spectra were recorded on a FT-IR JASCO 680-PLUS spectrometer using KBr pellets. UV-visible spectra were recorded with a JASCO 7580 UV-Vis-NIR spectrophotometer. Cary Eclipse fluorescence spectrophotometer was the secondhand for fluorescence emission. A 500 MHz Bruker spectrometer operating at 500.13MHz for ^{1}H and 161.97MHz for ^{31}P was referenced to H_3PO_4 (85%) for $^{31}P\{^{1}H\}$-NMR spectra, which were obtained in $CDCl_3$. For viscometric titrations, a cannon Fenske routine viscometer was used in a thermostatic water bath at 298 °K. Cells were cultivated in the Dulbecco's Modified

Eagle Medium (DMEM) supplemented in the activated fetal bovine serum (FBS). 5 mM L-glutamine, 100 μg.ml^{-1} streptomycin, and 100 U.ml^{-1} penicillin were used. Afterward, the cell lines were grown in a humidified atmosphere containing 5% CO_2 at 37 °C. Elemental analyses were performed on a Leco, CHNS-932 apparatus. The Tm spectra were recorded on a Varian BioCary-100 UV–Vis spectrophotometer using a 1 cm path length cell. CD spectra were recorded on an Aviv Circular Dichroism Spectrometer, the model 215 (USA), using a cylindrical cuvette with 0.1 cm path length.

2.3. Synthesis of compounds

1. Synthesis of [Pd(ClCH$_2$COCH(PPh$_3$)L)]Cl, L= PPh$_3$ (1)

First, the phosphorus ylide, [$PPh_3CH_2C(O)CH_2Cl$][Cl], was prepared according to our previous study [1]. Then, palladium (II) acetate (0.25 mmol, 0.053 g was added to a solution of mono-phosphonium salt [$PPh_3CH_2C(O)CH_2Cl$][Cl] (0.5 mmol, 0.194 g) in 15 mL of methanol and the resulting solution was stirred at room temperature for 24 h. The resulting solution was concentrated by reducing the solvent in vacuum to 2 mL. N-hexane (15 mL) was then added to separate [$Pd(ClCH_2COCHPPh_3)(\mu\text{-}Cl)]_2$ as an orange solid washed with diethyl ether, collected and air-dried. After that, PPh_3 (0.2 mmol, 0.052 g) was added to a solution of [$Pd(ClCH_2COCHPPh_3)(\mu\text{-}Cl)]_2$ (0.1 mmol, 0.098 g) in dichloromethane (15 mL). The resulting mixture was stirred at room temperature for 12 h. The suspension formed was filtered off, washed with diethyl ether, and dried to give 5 as a yellow powder.

Yield: 85%; IR (KBr, cm^{-1}): ν(C=O): 1663 cm^{-1}, ν (P-C) = 650-750 cm^{-1}. ^{1}H NMR (400.13MHz, DMSO-d_6, ppm): δ 4.5 - 4.7 (d, 2H, CH_2), δ 4.9 (t, 1H, CH), δ 7.2-7.9 (m, 29H, aromatic), $^{13}C\{^1H\}$ NMR (DMSO-d_6, ppm): δ = 37.3 (d, $^1J_{pc}$ = 56 Hz), 49.24 ($C_{aliphatic}$), 119.04, 121.16, 121.26, 122.34, 123.43, 123.62, 124.25, 125.17, 126.05, 126.35, 126.64, 127.37, 128.63, 129.14, 129.46, 129.72, 131.06, 131.27, 131.60, 131.72, 132.05, 132.22,

133.39, 133.45, 135.54, 135.66, 135.78, 135.83, 137.14, 137.20, 138.38, 138.80, 141.72, 146.46, 150.67, 153.30 ($C_{aromatic}$), 194.92 (s, CO), ^{31}P {^{1}H} NMR (DMSO-d_6, ppm): δ ~ 17 (s, 1P, CHP), 31 (s, 1P, PdP), Elemental Anal. Calcd. For $C_{39}H_{32}Cl_2OP_2Pd$: C, 62.01; H, 4.11%. Found: C, 61.92; H, 3.98%.

2. Synthesis of [Pd(ClCH$_2$COCH(PPh$_3$)L)]Cl, L=Py (2)

Pyridine (0.2 mmol, 0.016 g) was added to a solution of [Pd(ClCH$_2$COCHPPh$_3$)(μ-Cl)]$_2$ (0.1 mmol, 0.098 g) in dichloromethane (15 mL). The resulting mixture was stirred at room temperature for 12 h. The suspension formed was filtered off, washed with diethyl ether, collected, and dried to give a brown powder.

Yield: 80%; IR (KBr, cm^{-1}): ν (C=O):1668 cm^{-1}, ν (C-N) = 1602 cm^{-1}, ν (PC) = 650-750 cm^{-1}. ^{1}H NMR (400.13MHz, DMSO-d_6, ppm): δ 4.3 - 4.4 (d, 2H, CH_2), δ 4.5 (t, 1H, CH), δ 7 - 8.1 (m, 19H, aromatic), ^{13}C{^{1}H} NMR (DMSO-d_6, ppm): δ = 37.5 (d, $^{1}J_{pc}$ = 57 Hz), 49.35 (Caliphatic), 119.15, 121.44, 124.32, 125.64, 126.07, 127.37, 129.42, 129.65, 130.05, 130.87, 132.75, 133.17, 133.55, 135.46, 135.79, 138.30, 140.64, 141.77, 142.09, 144.18, 145.38, 151.21, 154.56 (Caromatic), 195.44 (s, CO), ^{31}P {^{1}H} NMR (DMSO-d_6, ppm): δ ~ 17 (s, 1P, CHP), Elemental Anal. Calc. For $C_{26}H_{22}Cl_2ONPPd$: C, 55.02; H, 4.02; N, 2.05%. Found: C, 54.94; H, 3.82; N, 1.96%.

2.4. X-ray crystallography

X‑ray diffraction data collection was carried out at 296 K using the X-scan technique and the X-RED32, developed by Stoe & Cie, 2002 package. The single crystal structure was solved by direct methods and refined by employing SHELXL-2016/6 (Sheldrick, 2016) program and using the ORTEP crystallographic software package. Table S1 shows the corresponding crystallographic data.

2.5. Studies of DNA binding

For DNA-binding studies, first, a stock solution of CT-DNA was prepared in the Tris-HCl buffer (5 mM Tris-HCl, 50 mM NaCl at pH 7.2) and stored at 4 °C. Then electronic absorption spectra were recorded in the 200-400 nm range using ε_{260} = 6600 M^{-1} cm^{-1} [25]; this was done by increasing 20 µl of CT-DNA to the complexes **1** and **2** solutions in the Tris buffer at room temperature. Each sample was retained for 5 min to reach equilibrium before recording the UV‑visible spectrum by electronic absorption measurement and fluorescence quenching experiments. In addition, the stock solution of CT-DNA was prepared in the Tris-HCl buffer (5 mM Tris-HCl, 50 mM NaCl at pH 7.2) and stored at 4 °C. Concentrated stock solutions of Pd complexes were prepared by dissolving them in DMSO and diluted with the buffer to develop the vital suitable concentrations in all experiments. The final DMSO concentration did not exceed 0.13% v/v and our complexes displayed good stability, as tested by electronic absorption spectrometry. All DNA-binding studies were done at room temperature by electronic absorption spectroscopy and fluorescence spectroscopy measurement. The test was done in the case of artificial model and differentiated with the real system biological environment of blood. Also, in our complexes, the ylide ligand could do the penetration phenomenon in the cell membrane because of its hydrophobic nature due to hydrolysis, but Pd remained in the aqueous solution [26].

2.6. Studies of protein binding

The fluorescence quenching of the tryptophan remainder of BSA, via the Pd complexes as a quencher, with variable complex/BSA molar ratios was proved in the range of 285-485 nm, at room temperature, and in the Tris buffer at 343 nm. In addition, titration of BSA and the marker compounds with the complexes was done to investigate the complex‑

BSA interaction by the existing BSA site markers, site I (Eosin-Y), site II (Ibuprofen), and site III (Digoxin).

2.7. Molecular docking of complexes with bio-macromolecules

Molecular docking simulation was performed in this study in order to survey the non-covalent interactions between the new synthesized complexes with BSA and DNA. Also, the binding affinity and the binding region of these complexes with bio-macromolecules was considered by the docking procedure. Free binding energy (ΔG) between complexes and macromolecules was calculated via molecular docking simulation. To prepare the complexes structures as ligands, the three dimensional structure of the pph3 complex (complex **1**) was obtained by converting the CIF file to PDB file using Open Babel 2.3.2 software [27]. The chemical structure of pyridine containing complex (complex **2**) was prepared using the Gauss View 5.0 software. Molecular energy optimization of this complex structure was performed using Gaussian 09 software (Quantum Chemistry package), by employing the density functional theory (DFT) method with Becke's three-parameter hybrid functional (B3LYP) through the 3-21G basis set. Crystallographic structures of BSA and DNA as the receptors were selected from the RCSB protein data bank *(http://www.pdb.org)*. The BSA (PDB ID: 4F5S) with 2.47Å resolution and DNA (PDB ID: 2GVR) with the 1.65Å resolution of the self-complementary dodecamer 5'-d(CGCGAATTCGCG)-3' were chosen for docking simulation. Excessive molecules such as hetero atoms and waters were removed. Free molecular docking packages, Auto Dock 4.2.6 and Auto Dock Tools 1.5.6, were used in this study for docking simulation [28,29].

The PDB formats of complexes and bio-macromolecules were modified by computing polar hydrogens, Gasteiger and Kollman charges. At first, the blind docking approach was

employed to probe the possible binding sites with the highest binding energy affinity of complexes to the three dimensional structure of BSA and DNA [30]. Finally, focus docking was done on the best binding site. The grid boxes dimensions size at the grid points in x*y*z directions were set to 60*60*60 $Å^3$ with 0.375 Å grid spacing for both bio-macromolecules. The Lamarckian genetic algorithm method with the assigned 100 numbers run of genetic algorithm has been mentioned [29]. All parameters default values in Auto Dock Tools software were adjusted in this docking study.

2.8. Cytotoxicity assay

The 3-(4,5-dimethylthiazol-2-yl)-2,5-diphenyltetrazoliumbromide (MTT) assay was used to calculate the cytotoxic activity of the complexes **1** and **2** against Jurkat and K562 cancer cell lines. This test was carried out using a fixed concentration of tumor cells that had been scattered in the wells of a 96-well plate with variable concentrations of the synthesized complexes (0–100 mmol dm_3) and incubated for 48 h. (37°C, 5% CO_2, 95%air humidified). Next, 20 µl of the MTT solution (5 $mg.ml^{-1}$in phosphate buffer solutions) was added to each well and the plates were incubated for 4 h at 37 ^{0}C. Afterwards, 100 µl of the medium including MTT was quietly substituted by dimethyl sulfoxide (DMSO) and pipetted to dissolve any formazan crystal wrought. Finally, after the complete dissolution of the dye, the optical density (OD) was measured at 560 nm by means of an enzyme-linked immunosorbent assay (ELISA) plate reader (Bio-Tek's ELx808, USA). The ratio inhibition of the cells was measured as follows: % Inhibition= 100 - [(test OD/non-treated OD) × 100]. Non-treated cultures in all treatments consisted of only the DMSO solvent at a concentration identical to those in the test wells. IC_{50} (value of 50% maximal inhibitory concentration) was determined using the non-linear regression of concentration response curves [31,32].

2.9. Cell cycle analysis by flow cytometry

The effects of ylide ligand and complexes **1** and **2** on cell cycle changes in Jurkat and K562 cells were studied by propidium iodide staining using flow cytometry. Cells at concentration of 1×10^6/ml/well were seeded in 24-well plates in triplicate and treated with the compounds at concentrations equal to their IC_{50} values calculated from the results of MTT cytotoxicity assay. After 48 h of culture at 37°C in a CO_2 incubator, the cells were harvested and then permeable with 1ml hypotonic solution containing sodium citrate (1%) and triton X-100 (0.1%). Then propidium iodide (Sigma Aldrich, Steinheim, Germany) at final concentration of 50 µg/ml was added. After 2 h incubation at 4 °C, cells were examined for the intensity of fluorescent dye by flow cytometry (Becton Dickinson, San Diego, CA) in FL2 channel. The results were analyzed by FlowJo software version 7 (TreeStar Inc, Ashland, OR). Cells treated with cisplatin were considered as positive control and those treated only with DMSO (untreated) considered as negative control.

3. Results and discussion

3.1. Synthesis and spectroscopic characterization

In this work, the reaction of mono phosphonium salt (A) (scheme 1) with palladium(II) acetate in a 2:1 ratio in methanol and at room temperature for 24 h resulted in the chloro-bridged dinuclear complex $[Pd\{C(H)PPh_3C(O)CH_2Cl\}(\mu\text{-}Cl)(OAc)]_2$ (B) (scheme 1) [1]. The treatment of PPh_3 and Py with (B) (2 : 1 M ratio) in dichloromethane at room temperature for 12 h yielded yellow solids soluble in the DMSO solvent; their stoichiometry corresponded to cationic orthometalated derivatives $[Pd(ClCH_2COCH(PPh_3)PPh_3)]Cl$ (complex **1**) and $[Pd(ClCH_2COCH(PPh_3)Py)]Cl$ (complex **2**) in good yields. So, complexes were characterized using FT-IR and NMR spectroscopy methods. The crystal structure of the

complex **1** was addressed by X-ray crystallography studies (Figure 1). The spectroscopic data of **2** was in accordance with the similar structure. The IR spectrum of the complexes **1** and **2** showed strong bands at 1630-1670 cm^{-1} that were assigned to ν (C=O) stretching bands. The C-bonding of the ylide-phosphonium salt could be concluded from the IR spectrum, since a decrease in the C=O stretch was observed [33,34]. Furthermore, three bands at 650-750 cm^{-1} were due to ν (P–C), lower than the parent phosphonium salt 1[35] because of the elimination of electron density in the P–C bond, confirming the coordination of the ligand to Pd through the carbon, not through oxygen; this was confirmed for the complex **1** by X-ray diffraction. Additionally, the IR spectra of the complex **2** showed ν (C=N) as a strong band at 1602 cm^{-1}. Also, the strong bands at 1580 and 1335 cm^{-1} were due to asymmetric and symmetric ν (COO) stretching bands, respectively, which were consistent with monodentate acetate, and the band at 470 cm^{-1} was due to ν (Pd-OAc) [36].

The ^{1}H NMR spectra of **1** and **2** showed signals for the PC(H) at 4.5-4.9 ppm, which were shifted up field in comparison with the parent phosphonium salt (5.5), similar to other C-coordinated phosphonium ylide complexes [34]. Furthermore, the aromatic protons were observed in the ~7-8 ppm range and signals for the protons of CH_2 were assigned at 4.3-4.7 ppm. In ^{31}P {1H} NMR spectra of **1** and **2**, signals due to PC(H) groups were 17 ppm and at 23 ppm for extra phosphonium salt, so we purified to remove it. Also, the signal due to PdP for the complex **1** was assigned at 31 ppm.

Scheme 1

3.2. Molecular structure of the complex

Single X-ray crystallography was utilized to study the synthesized complexes. The ORTEP view of the complex **1** is displayed in Figure 1. Table 1 represents the selected bond

distances and angles. The data showed that the complex **1** was crystallized in the monoclinic space group, with four molecules within the unit cell. Distortion from the regular square planar geometry was indicated by the bond angles around the Pd center. The Pd_C_{aryl} bond distance (2.001(4) Å) was within the range generally reported for C,C-orthopalladated complexes [37,38].

Bond lengths and angles at Pd were slightly distorted (C1—Pd) 2.001(4), (P2—Pd) 2.3108(12), (Cl1—Pd1) 2.3828(12), (C37—Pd1) 2.144(4), (P2—Pd1—Cl1) 94.91(5), (C1—Pd1—C37) 85.44(16). The stabilized resonance construction for the parent ylide-phosphonium was destroyed because of complexation; therefore, the C1-C2 bond lengths (1.408(5) Å) were slightly longer than the corresponding distance found in similar non complexed phosphoranes (1.407(8)Å, suggesting that this bond has been relatively week. Although the C38-O1 bond lengths (1.216(6)) Å were shorter than those observed in a similar ligand (1.256(2) Å) [39], they showed that the C-bonding of the ligand kept the charge density at C and discontinued the conjugation.

Figure 1

Table 1

3.3. Stability of complex in solution

The electronic spectra of the complexes displayed a band around 250 nm which could be attributed to the n-π* electron transition of triphenylphosphine groups in the structure of complexes. The stability of the compounds in the DMSO solution was tested by electronic absorption (S2). No changes were observed in absorbance after incubating the synthesized

complexes in DMSO with increasing time to 10 days; this confirmed the stability of the complexes and the preservation in solution.

3.4. DNA-binding studies

3.4.1. Electronic absorption investigations

One of the common, sensitive, reproducible and simple techniques to study the binding mode of DNA with metal complexes is electronic absorption spectrometry [40]. The electronic absorption spectra of the complexes were recorded for a stable concentration of the free metal complexes [6×10^{-5} M] by increasing CT-DNA; the results are shown in Figure 2, which represents the mode of interactions [41]. The absorption band was around 250 nm for the complexes, which could be assigned to the intra ligand transition [42]. Thus, the titration data obtained by adding DNA to the complexes showed the decrease of absorbency with no shift of the absorption peak in the UV-vis spectrum, thereby confirming that the complexes/CT-DNA interactions were not intercalated. To determine the binding power of the Pd complexes along with CT-DNA, the intrinsic binding constant, K_b, was calculated via the Wolfe-Shimmer equation (1): [43]

$$[DNA]/(\varepsilon_a - \varepsilon_f) = [DNA]/(\varepsilon_b - \varepsilon_f) + 1/K_b(\varepsilon_b - \varepsilon_f) \quad (1)$$

,where [DNA] is the DNA concentration, and ε_a, ε_f and ε_b correspond to A_{obs}/[complex], the destruction coefficients for the free complex, and the entirely attached form of the complex, respectively. A plan of $[DNA]/(\varepsilon_a - \varepsilon_f)$ vs. [DNA]gave a slope and an intercept fit equal to $1/(\varepsilon_b - \varepsilon_f)$ and $1/K_b(\varepsilon_b - \varepsilon_f)$ (Figure 2). The intrinsic binding constant (K_b) could be obtained from the ratio of the slope to the intercept [44]. The calculated K_b value of the complexes was about 4.9×10^6 M^{-1} for the complex **1** and 2.3×10^6 M^{-1} for the complex **2** at 298 K, indicating the high binding ability of the complexes with CT-DNA. DNA has different hydrogen bonding sites in its grooves. Therefore, the ylidic ligand would encourage the intercalation of the phenyl group in the groove mode. Free energy (ΔG) of compound-DNA

complexes could be achieved from the amounts of binding constant (K_b) through the van't Hoff equation (2): [45]

$$\Delta G = - RT \ln K \quad (2)$$

Binding constants are typical of the stability of compound-DNA complexes, while free energy shows the spontaneity/non-spontaneity of the compound-DNA binding. The free energy of the complexes **1** and **2** was -9.13 $Kcalmol^{-1}$ and -8.7 $Kcalmol^{-1}$, respectively, and the negative values showed the spontaneity of the compound-DNA interaction.

Figure 2

3.4.2. Fluorescence emission titration

To study whether the type of the binding of the Pd complexes to DNA was the groove or intercalative mode, the comparative methylene blue (MB) displacement assay was used. The emission intensity of MB was quenched by the addition of CT-DNA [46]. This emission quenching process also indicated the alterations in the excited state electronic structure as a result of the electronic interactions in the MB-DNA complexes [47]. Figure 3 shows that the fluorescence intensity of MB-DNA was increased by adding the complexes. This revealed that the complex was bound to the base pairs of DNA [48]. The Fluorescence intensity of the MB probe molecule ([DNA]/[MB] = 10) at 680 nm was slightly increased by adding the two complexes **1** and **2** to DNA; this established that the DNA/Pd complexes interaction was in the partial intercalative mode. Moreover, from the plot of F_0/F *vs*. [complex], the apparent DNA binding constant (K_{app}) was calculated using the following equation: [49]

$$K_{MB}\,[MB] = K_{app}\,[complex] \quad (3)$$

,where K_{MB} is the DNA binding constant of MB, [MB] is the concentration of MB, and [complex] is the concentration of the complex at 50% quenching of the DNA-bound methylene blue fluorescence emission intensity. The value of K_{app} was 1.2×10^5 and 1.04×10^5 M^{-1} for the complexes **1** and **2,** respectively, which was slightly less than the

binding constant of the classical intercalators and metallointercalators (10^7 M^{-1}) [50], revealing that the compounds were bound to DNA in the groove binding mode.

Figure 3

3.4.3. CD spectroscopy

Circular dichroic (CD) studies are useful in identifying the changes in the morphology of DNA. CD spectra of DNA showed two characteristic bands; the first one at 245nm was related to the helicity of the right handed B-form and the second one at 260-285 nm was due to base stacking [51]. This method could be useful in monitoring the changes in the DNA structure in the presence of the synthesized complexes as drugs in solution, resulting in some changes in the intensity and wavelength of its CD spectra [52]. Thus, less or no perturbation was displayed by the simple groove binding and the electrostatic interaction of small molecules with DNA; on the other hand, increasing the intensities of both bands demonstrated that the stabilization of the right handed B conformation of CT-DNA could be improved by intercalation, as observed in the classical intercalator methylene blue [53,54]. The CD spectra of DNA in the absence and presence of complexes were recorded in the range of 230–330 nm at 25 ^{0}C using a bandwidth of 1 nm, a step interval of 1 nm, an average time of 1 second, and the resolution of 1 nm. For the complexes **1** and **2**, the CD spectra of DNA exhibited changes in intensity by the addition of complexes, without any changes in the wavelength (Fig. 4). The less decrease of the negative bands and the decrease of the positive bands demonstrated that the two complexes were bound to the DNA via groove mechanism with the partial intercalative mode in the DNA-base pairs [55-57].

Figure 4

3.4.4. Thermal denaturation studies

DNA denaturation studies can be used to distinguish the nature of the interaction of the complexes with DNA via the groove or intercalation mode. The melting temperature (Tm) is related to the stability of the double helical structure of DNA [58], which is raised sharply in the presence of metallo-intercalators. The small shift in the Tm value of CT‐DNA could propose non‐classical modes such as partial intercalation, groove binding, and/or surface binding modes [59,60]. The melting curves of CT‐DNA in the absence and presence of the complexes are shown in Figure 5. The melting temperature of CT‐DNA was found to be 82 °C in the buffer. After the addition of the Pd(II) complexes, Tm was increased to 86.16 and 85.22 °C for the complexes **1** and **2**, respectively. Since increasing Tm in 4-12 °C range was due to the intercalation of the compounds into DNA base pairs and this range for non-intercalative binding mode was 0-4 °C, this amount for our complexes showed the possibility of the partial intercalation between the CT‐DNA and the two complexes [60].

Figure 5

3.4.5. Viscosity measurement

The DNA length (L/L_0) and relative viscosity (η/η^0) are measured by $L/L_0 = (\eta/\eta^0)^{1/3}$, where η and L are the specific viscosity and the molecular length of DNA at a gained complex/DNA ratio, respectively; also, η^0 and L_0 are the corresponding values for the alone DNA [61]. For an intercalated molecule, a hypothetical rise in the amount of DNA viscosity was considered because of the insertion between the DNA base pairs and the lengthening of the DNA double helix [62].

Additionally, the bounded molecules via the groove mechanism made minor or no effect on the viscosity of the DNA solution [63]. However, the viscosity of CT-DNA was not seriously

affected through the addition of the two complexes **1** and **2** (S3). This presentation suggested that the Pd complexes might be bound to DNA upon groove binding with a slight intercalative style.

3.5. Protein binding experiments

Serum albumins are well known for binding to small aromatic groups mainly containing part of the protein in blood plasma; they play a significant part in drug delivery. Thus, to identify the possible binding interaction between BSA and complexes, emission titration and absorption experiments were used at the ambient temperature.

3.5.1. Fluorescence spectroscopy studies

Tryptophan emission quenching experiments were used to study the interaction of the complex with the protein; f tyrosine fluorescence is ionized, it has been totally quenched and phenylalanine has a very low quantum yield [64]. The effect of the Pd complexes on the BSA fluorescence emission can be seen in Figure 6. The intensities of the fluorescence emission of BSA were decreasedregularly with the addition of the two complexes **1, 2**, which established the interaction between the complex and BSA. Stern–Volmer equation (4) has also been used in the data analysis of the fluorescence quenching and the quenching ability of the complexes: [65]

$$F_0/F = 1 + k_q \tau_0 [Q] = 1 + K_{SV}[Q] \quad (4)$$

, where F_0 and F are the fluorescence powers in the absence and presence of the complexes as the quencher, respectively, [Q] is the concentration of the quencher, K_{sv} is the Stern–Volmer quenching constant, τ_0 is the average life time of the fluorophore without quencher, and k_q is the bimolecular quenching rate constant. In this research, the value of K_{sv} was 1.58×10^6 M^{-1}

and 1.56×10^{6} M^{-1} for Pd complexes **1** and **2**. Since the value of τ_0 for tryptophan fluorescence is 2×10^{-8} s [63], the quenching rate constant, k_q, can be measured via the following equation:

$$k_q = K_{SV}/\tau_0 \quad (5)$$

The obtained values for k_q were 79×10^{12} and 78×10^{12} $M^{-1}S^{-1}$ for the complexes **1** and **2** respectively. Also, the highest concentration of k_q for diverse quenchers with the biopolymer is 2×10^{10} $M^{-1}S^{-1}$ [66]. Therefore, the amount calculated was greater than k_q of the scatter procedure. This exhibited that a static quenching mechanism was operative [67].

Figure 6

3.5.2. Determination of the binding constant (K_b) and the number of binding sites (n) on BSA

The number of binding sites and the binding constant for the static quenching interaction can be calculated according to the following equation: [68]

$$\text{Log } (F_0 - F)/F = \log K_b + n \log [Q] \quad (6)$$

, where K_b is the binding constant of the complex with protein and n is the average number of the binding sites per albumin molecule. The plot of log $[(F_0 - F)/F]$ vs. Log [Q] is exposed in Figure 6. K_b and n can be determined from the slope of such a plot. The values of K_b and n at 298 K were 1.58×10^{6} M^{-1} and 0.99 for the complex **1** and 1.56×10^{6} M^{-1} and 0.98 for the complex **2**. The values of n point were such that there was only one class of binding site for the two Pd complexes on BSA.

3.5.3 Determination of site selective binding

BSA crystal structure comprises three distinct drug binding domains (sites I, II, and III) [69]. Sites I, II and III in serum albumin are suggested to correspond to Eosin-Y, Ibuprofen and Digoxin binding sites, respectively [70]. The experiments, due to competition, were done through Eosin-Y, Ibuprofen and Digoxin to achieve the drug binding sites. In this test, the BSA/site marker concentration proportion was 1:1 (6×10^{-6} M: 6×10^{-6} M). Figure 7 shows that by the addition of the site specific probe into the BSA solution, the fluorescence intensity was significantly decreased. Thus, Eq. (6) was used for the calculation of the binding constants (Table 2). So, in the presence of Eosin-Y probe, the binding constant of the complexes **1** and **2** was decreased. The results pointed to the competition of Eosin-Y and Ibuprofen with the complexes. Thus, the complexes **1** and **2** could bind to the site I and the site II of serum albumin, respectively.

Figure 7

Table 2

3.6. Molecular docking

3.6.1. Molecular docking study of the complexes with BSA

The lowest free binding energy (ΔG) calculated for the complex **1** and the complex **2** to BSA was -7.19 $Kcalmol^{-1}$ and -10.68 $Kcalmol^{-1}$ in docking simulation, respectively. In order to study the fluorophore residue (Tryptophan) quenching in the presence of complexes , the distance between the best docked conformer of the complex **1** and the complex **2** and Trp134 and Trp213 as a fluorophore residue of bovine serum albumin was measured. The length between the complex **1** and Trp134 was 19.7Å and that between the complex **1** and Trp213 was 22.5Å (Fig.8A). Also, these distances for the complex **2** were 27.0Å and 20.0Å for Trp134 and Trp213, respectively (Fig.9A). The obtained distances for both complexes

were less than 80 Å. In order to do the quenching of protein fluorescence emission, this distance was enough in the presence of the ligand (in this study, the complex **1** and the complex **2**). Docking simulation confirmed our findings by experimental quenching studies [71,72]. For the better study of the interacted residues with the new synthesized complexes, all docking conformations between the complexes and BSA were examined. Residues interacted with complex **1** included: Thr2, His3, His9, Arg10, Lys12, Asp13, Asp236, Lys239, Asp254, Asp255, Ala257, Asp258, Leu259 and Lys261. In Fig.8B, 8C and 8D, the interaction of the complex **1** with BSA is represented by three and two-dimensional modes, respectively. AutoDookTools has the ability to present the non-covalent interactions such as hydrogen bond, π–π stacking and π-cation interactions between the receptor residues and the ligand from the output file of the docking procedure. The receptor residues and the ligand must have close contacts with each other for these types of interactions. The amino functional group of Arg10 from BSA participated in hydrogen bond formation via the methoxy functional group of the complex **1**. The measured distance between the hydrogen atom and the oxygen atom in hydrogen bonding was 2.1Å (Fig.8B). Due to presence of aromatic rings in the complex **1** molecular structure, the formation of other non-covalent interactions, especially π-cation interaction and π–π stacking interaction by the complex **1** occurred. Lys261 and His3 are the residues with which the complex **1** have π-cation and π–π stacking interaction, respectively. The distances between these residues and the aromatic ring of the complex **1** that participated in the interactions were 3.6Å and 5.8Å for the π-cation interaction and the π–π stacking interaction, respectively (Fig.8B and Fig.8C). According to the best docking conformer results, the complex **1** had hydrophobic interactions with His3, His9, Lys12, Asp13, Asp254, Asp258, and Lys261. (Fig.8D (spoked arcs)).

Complex **2** and BSA interactions were analyzed for all docking conformations. The residues participated in this reaction were found. The residues that interacted with the

complex **2** included: Glu100, Leu103, Ser104, Ile202, Gln203, Lys242, Cys245, and His246. Interactions of the complex **2** with BSA are demonstrated by the three and two- dimensional mode in Fig.9B and Fig.9C, respectively. According to the best docking conformer results, the complex **2** had hydrophobic interactions with Leu103, Ser104, Ile202, Gln203, Lys242, Cys245, and His246 (Fig.9C (spoked arcs)). Pyridine heterocyclic ring in the complex **2** structure facilitated the formation of the hydrogen bond, where the hydrogen bond was formed between the oxygen (OE1) of Glu100 and the nitrogen of pyridine (Fig. 9C (green dashed line)). Also, the Pd atom of the ligand was interacted (external bond) with the side-chain of Glu100 by oxygen (OE1) (Fig. 9C (purple line)). The ability of the external bond formation as well as hydrogen bonds due to the nitrogen of the pyridine ring by the complex **2** showed the high affinity of the complex **2** to BSA rather than the complex **1** in a molecular docking study.

Figure 8

Figure 9

3.6.2. Molecular docking study of the complexes with DNA

The calculated lowest free binding energy (ΔG) of the molecular docking simulation of the complex **1** and the complex **2** with DNA was -7.07 $Kcalmol^{-1}$ and -12.50 $Kcalmol^{-1}$, respectively. The interaction between DNA and both synthesized complexes was of the groove type, as determined from docking results analyses (Fig.10A and Fig.11A). The other docked conformers revealed the partial intercalation mode, supporting the experimental absorption spectroscopy findings in this study. Analyzing f all conformations from docking between DNA and the complex **1** identified the main nucleotides participating in the

interaction with the complex. These nucleotides included: DG2, DC3, DG4, DA5, DA6, DT7, DT8, DG16, DA17, DA18, DT19, and DT20. Hydrogen bonding was formed between the methoxy functional group of the complex **1** and the exocyclic amino groups of DG4, DA5, DA6, DG16, DA17, and DA18 nucleotides. The measured distance between the donor (N) and acceptor (O) atoms in hydrogen bonding between DG4 and the complex **1** was 2.8Å (Fig.10B). Purines nucleotides played a major role in hydrogen bonding formation with the complex **1**. The presence of aromatic rings caused the formation of the non-covalent π–π stacking interaction between the nucleotides aromatic rings and the phenyl groups of the complex **1**. The nucleotides taking part in non-covalent π–π stacking interactions were DG4, DA5, DA6, DG16, DA17, and DA18 (Fig.10B and Fig.10C). The three-dimensional interaction between the complex **1** and DNA is shown in these figures. Based on these figures, the length of the non-covalent π–π stacking interaction between the complex **1** and DA5 and DA6 was 4.8Å and 5.4Å, respectively (Fig.10B). In addition, the π–π stacking interaction distance between DA17 and DA18 and the complex **1** was 4.5Å and 5.2Å, respectively (Fig.10C). The two dimensional representation of the complex **1** and DNA interaction is demonstrated in Fig.10D. According to this figure, DA17, DA18 and DT19 had the hydrophobic interaction with the complex **1** (spoked arcs in Fig.10D).

All conformers from the molecular docking study between the complex **2** and DNA indicated that main nucleotides with which the complex **2** had interacted. They were DT8, DC9, DG10, DC11, DG12, DA17, DA18, DT19, and DT20 nucleotides. In Fig11.B, the three-dimensional interaction between the best docked conformer of the complex **2** and DNA is indicated. The two-dimensional representation of the interaction between the complex **2** and DNA is depicted in Fig.11C. The complex **2** had hydrophobic interaction with DT8, DC9, DA18, DT19, and DT20 nucleotides (spoked arcs in Fig.11C). Like the interaction of the complex **2** with BSA, the complex **2** could form hydrogen bond via the nitrogen of the

pyridine ring with the oxygen (OP1) of DG10 (Fig. 11C (the green dashed line)), and the palladium atom could form the external bond with the oxygen of DG10 (Fig. 11C (purple line)).

Totally, the external bond formation via palladium atom, van der Waals interactions, and strong hydrogen bonds formation by the nitrogen of the pyridine ring caused the complex **2** to have high affinity binding for both bio-macromolecules in docking studies. The outstanding tendency of the complex **2** to DNA proposed the usage of this palladium as a new synthesized complex serving as an anticancer. All non-covalent interactions (hydrogen bonding, π-cation and π–π stacking interactions) distances between BSA and DNA with the complex **1** are shown in the three- dimensional scheme in Fig 8 (B,C) and Fig 10 (B,C), and in Table 3.

Figure 10

Figure 11

Table 3

3.7. Selective cancer cytotoxic activity

Cytotoxic activity of the ylide ligand and the complexes **1** and **2** was evaluated against human leukemic T cell (Jurkat) and chronic myelogenous leukemia (K562) cell lines. The viability of the treated cell lines was determined after 48 hours via a standard bioassay, by the MTT-dye reduction method. The cytotoxic activity of cisplatin as the standard reference was evaluated for the comparison purposes.

As shown in Figure 12, both the ligand and the complexes **1** and **2** could dose-dependently decrease the viability of Jurkat and K562 cell lines at the evaluated doses. The complex **1** at the doses ranged from 1 to 100 µM, exerting 10% – 91% and 10.5% - 95% toxicity against K562 and Jurkat cancer cells, respectively. Additionally, the complex **2** at the doses ranged

from -1 to 100 µM, exerting 20% – 98% and 2.5% - 95% toxicity against K562 and Jurkat cancer cells, respectively. The ligand at the same concentrations was found to exert 2.2% - 98% cytotoxic effect against the K562 cell line, while showed 3.2% – 93 % cytotoxicity against the Jurkat cell line. The cytotoxicity data, expressed as IC_{50} values, are presented in (Table 4). IC_{50} (µM) values of cisplatin, as the reference anticancer compound and a standard drug on K562 and Jurkat cells, are shown; the results for the ligand and complexes in comparison with the reference were noticeable. The results implicated that the ligand and the two complexes **1** and **2** could highly and significantly exert a cytotoxic effect against K562 and Jurkat cancer cell lines. According to the IC_{50} values, the cytotoxicity of **1** against K562 cells was more than **2,** probably due to the presence of the triphenylphosphine moiety in its molecular structure, could improve the cytotoxic activity [73]. Also, the IC_{50} value of ligand in that cells is near to cis-platin, but for complexes **1** and **2** these values had been better. No considerable difference in cytotoxicity of the compounds against Jurkat cells was detected, suggesting that Complexes **1** and **2** may do not increase the cytotoxicity of the ligand against this cell line, or the difference between the biological nature and origin of the tumor cell lines has resulted in their different sensitivity to the compounds. The results have been supported by the other in vitro studies reporting the cytotoxic activity of the ylide complexes against cancer cell lines [74,75].

Figure 1

Table 4

3.8. Effects of compounds on cell cycle

In order to determine the effects of ligand and Pd complexes on cell cycle progression, Jurkat and K562 cell lines were cultured in the presence of the compounds for 48 h and then were

stained with propidium iodide to be analyzed for DNA content by flow cytometry. As shown in Figure 13, the ligand and two complexes **1** and **2** have significantly induced apoptosis in treated cells. Cisplatin as positive control induced accumulation of 42.7±6.5% of Jurkat and 41.2±8% of K562 cells in subG1 phase (apoptotic cells) compared to the negative controls (<4.1%). The percentages of compound-treated Jurkat cells underwent apoptosis were 41.1±3.9 (ligand), 44.9±5.8 (complex **1**) and 55.2±6.2 (complex **2**). Similarly, treatment of K562 cells with the compounds significantly shifted the main population of cells toward the subG1 phase. The complexes simultanously with inducing accumulation of cells in subG1 phase, have efficiently decreased the percentage of Jurkat cells (27.3±2.3%) and K562 cells (27.4±8.2%) in G0-G1 phase as compared to that in negative control (≈51-55%) suggesting an induction of subG1 arrest in the cells. A representative example of flow cytometry analysis of cell cycle distribution in treated Jurkat and K562 cells is shown in Figure 14.

Thus, the effects of ylide and Pd complexes on cell cycle changes were determined by the propidium iodide staining using flow cytometry. Propidium iodide is a fluorescent dye with the ability to enter the cells and bind DNA. Evaluation of cell cycle phases in treated cells showed that the ligand and Pd complexes have decreased DNA content by inducing apoptosis and accumulation of cells in subG1 phase. The percentage of subG1 cells and decreased number of G0-G1cells treated with Pd complexes were comparable to those treated with cisplatin. Reduction in the number of G0-G1 cells suggested their ability to induce subG1 arrest.

Figure 2 Figure 3

3.9. Energy transfer between Pd complexes and BSA

A non-destructive spectroscopic procedure for monitoring the proximity and the relevant angular orientation of fluorophores is fluorescence resonance energy transfer (FRET) [76]. It has been used to measure the donor-acceptor distance in macromolecular and biological systems. In addition, the overlap between the excitation band of the acceptor and the donor is significant and the distance between them is within 2–8 nm [77]. The efficiency of energy transfer (*E*) then depends on the distance, R_0, between the acceptor and the donor, as shown by the equation (7): [78]

$$E = 1- F/F_0 = (R_0^6) / (R_0^6 + r^6) \quad (7)$$

, where *r* is the distance between the donor and acceptor, and R_0 is the critical energy transfer distance at which 50% of the energy is transferred to the acceptor; it is defined by the following equation: [79]

$$R_0^6 = 8.8 \times 10^{-25} \kappa^2 N^{-4} \Phi J \quad (8)$$

In Eq. (8), κ^2 is the orientation space factor and $\kappa^2 = 2/3$ for the random orientation is as in the unsolidified solution. N is the ordinary deflected medium index in the range of wavelength with the significant spectra, Φ is the fluorescence quantum output of the donor, and J is the effect of the spectral overlay between the emission spectrum of the donor and the absorption spectrum of the acceptor (Figure 15) which could be obtained from the following equation: [80]

$$J = [\sum F(\lambda)\varepsilon(\lambda)\lambda^4\Delta\lambda] / [\sum F(\lambda)\Delta\lambda] \quad (9)$$

F (*λ*) is the modified fluorescence intensity of the donor in the wavelength array *λ* to *λ* +Δλ, and *ε* (*λ*) is the extermination constant of the acceptor at *λ*. In the present case, *n* = 1.336 and Φ= 0.15 [81]. Pursuant to equations (7)–(9), $J=3.66\times10^{-15}$, 1.13×10^{-14} $cm^3L\ mol^{-1}$, R_0 = 2.15, 2.6 nm, *E*=0.11, 0.12 and *r*=2.06, 2.01 nm for the complexes **1** and **2,** respectively. The mean distance between the donor and the acceptor was on the 2–8 nm range and $0.5R_0 < r < 1.5R_0$,

thereby indicating that the energy transfer from BSA to the Pd complexes might have occurred with high probability.

Figure 4

4. Conclusion

Two new orthometallated complexes were promoted under mild conditions by the reaction of $[Pd\{C(H)PPh_3C(O)CH_2Cl\}(\mu\text{-}Cl)(OAc)]_2$ with PPh_3 and Py as the chelating ligands, yielding the two mononuclear orthometallated complexes **1** and **2**. Single X-ray crystallography method was applied to characterize the structure of the complex **1,** showing a monoclinic geometry for the Pd atom. The DNA binding properties of the prepared complexes were checked out using fluorescence spectroscopy, electronic absorption, and viscometry measurements. The complex-CT-DNA interaction for the two complex **1** and **2** was via groove binding with the partial intercalation, according to the results. The quenching of BSA emission through the complex was of the static form, as shown by the reactivity toward BSA. Site marker competitive analysis showed that the two Pd complexes could bind to the BSA molecule in one site. The molecular docking studies also supported the above results and successfully verified the interaction mode of the complex with DNA and BSA. Cytotoxic activity of the Pd complexes against K562 and Jurkat cell lines demonstrated the potent effect against K562 and Jurkat cancer cell lines and confirmed the anti-tumor activity of Pd compounds. Cell cycle analysis showed that the complexes have significantly increased the proportion of subG1 cells and effectively reduced G0-G1 cells implying the effect of compounds on cell cycle arrest by decreasing cell DNA content and inducing cell death. The binding distances with BSA based on the Foster's theory illustrated that the energy transfer could occur from BSA to the ylide complexes.

Acknowledgements

This research was funded by Isfahan University of Technology (IUT). Crystallography was provided by the Faculty of Arts and Sciences, Department of Physics, Ondokuz Mayrs University.

References

[1] K. Karami, S. Amouzad, M. Hosseini-Kharat, C. Rizzoli, J. Coord. Chem. 66 (2013) 1774-1783.

[2] E.P. Urriolabeitia, Top. Organomet. Chem. 30 (2010) 15-48.

[3] E. Serrano, C. Valles, J.J. Carbo, A. Liedos, T. Soler, R. Navarro, E.P. Urriolabeitia, Organometallics. 25 (2006) 4653-4664.

[4] A. Kawachi, T. Yoshioka, Y. Yamamoto, Organometallics. 25 (2006) 2390-2393.

[5] K. Karami, S. Abedanzadeh, F. Yadollahi, O. Büyükgüngör, H. Farrokhpour, C. Rizzoli, J. Lipkowski, J. Organomet. Chem. 781 (2015) 35-46.

[6] K. Karami, S. Hashemi, J. Lipkowski, F. Mardani, A.A. Momtazi-borojeni, Z.M. Lighvan, Applied Organometallic Chemistry. 31 (2017).

[7] M.J. Hannon, J. Reedijk, Dalton Trans. 44 (2015) 3503-3504.

[8] A.R. Kapdi, I.J. Fairlamb, Chem. Soc. Rev. 43 (2014) 4751-4777.

[9] E. Chardon, G.L. Puleo, G. Dahm, S. Fournel, G. Guichard, S. Bellemin-Laponnaz, ChemPlusChem. 77 (2012) 1028-1038.

[10] K. Karami, M. Alinaghi, Z. Amirghofran, J. Lipkowski, Inorg. Chim. Acta. 467 (2017) 46-55.

[11] M.R. Shehata, M.M. Shoukry, M.S. Ragab, R. van Eldik, Eur. J. Inorg. Chem. 13 (2017) 1877-1887.

[12] F. Kaiser, A. Schmidt, W. Heydenreuter, P.J. Altmann, A. Casini, S.A. Sieber, F.E. Kühn, Eur. J. Inorg. Chem. 33 (2016) 5189-5196.

[13] D. Sarkar, P. Das, S. Basak, N. Chattopadhyay, J. Phys. Chem. B. 112 (2008) 9243-9249.

[14] B.L. Fei, W. Li, W.S. Xu, J.Y. Long, Q.B. Liu, W.Y. Sun, C.E. Anson, A.K. Powell, Eur. J. Inorg. Chem. 34 (2013) 5919-5927.

[15] K. Karami, M. Alinaghi, Z. Amirghofran, J. Lipkowski, A.A. Momtazi-borojeni. New J. Chem. 42 (2018) 574-586.

[16] K. Karami, M. Rafiee, Z.M. Lighvan, M. Zakariazadeh, A.Y. Faal, S.A. Esmaeili, A.A. Momtazi-Borojeni, J. Mol. Struct. 1154 (2018) 480-495.

[17] M. Anjomshoa, H. Hadadzadeh, M. Torkzadeh-Mahani, S.J. Fatemi, M. Adeli- Sardou, H.A. Rudbari, V.M. Nardo, Eur. J. Med. Chem. 96 (2015) 66-82.

[18] K. Karami, Z. Mehri Lighvan, H. Farrokhpour, M. Dehdashti Jahromi, A.A. Momtazi-borojeni, J. Biomol. Struct. Dyn. (2017) 1-17.

[19] P. Sathyadevi, P. Krishnamoorthy, E. Jayanthi, R.R. Butorac, A.H. Cowley, N. Dharmaraj, Inorg. Chim. Acta. 384 (2012) 83–96.

[20] F. Arjmand, P. Tewatia, M. Aziz, R.H. Khan, Med. Chem. Res. 19 (2009) 794-807.

[21] R. Esteghamat-Panah, H. Farrokhpour, H. Hadadzadeh, F. Abyar, H.A. Rudbari, RSC Adv. 6 (2016) 23913-23929.

[22] M.T. Behnamfar, H. Hadadzadeh, J. Simpson, F. Darabi, A. Shahpiri, T. Khayamian, M. Ebrahimi, H.A. Rudbari, M. Salimi, Spectrochim. Acta, Part A. 134 (2015) 502-516.

[23] M. Reichmann, S. Rice, C. Thomas, P. Doty, J. Am. Chem. Soc. 76 (1954) 3047-3053.

[24] G. Felsenfeld, S.Z. Hirschman, J. Mol. Biol. 13 (1965) 407-427.

[25] P. Sathyadevi, P. Krishnamoorthy, N.S. Bhuvanesh, P. Kalaiselvi, V.V. Padma, N. Dharmaraj, Eur. J. Med. Chem. 55 (2012) 420-431.

[26] D.C. Crans, K.A. Woll, K. Prusinskas, M.D. Johnson, E. Norkus, Inorg. Chem. 52 (2013) 12262-12275.

[27] N.M. O'Boyle, M. Banck, C.A. James, C. Morley, T. Vandermeersch, G.R. Hutchison, J. Cheminform. 3 (2011) 33.

[28] G.M. Morris, R. Huey, W. Lindstrom, M.F. Sanner, R.K. Belew, D.S. Goodsell, A.J. Olson, J. Comput. Chem. 30 (2009) 2785-2791.

[29] G.M. Morris, D.S. Goodsell, R.S. Halliday, R. Huey, W.E. Hart, R.K. Belew, A.J. Olson, J. Comput. Chem. 19 (1998) 1639-1662.

[30] C. Hetényi, D. van der Spoel, FEBS letters. 580 (2006) 1447-1450.

[31] M. Asadi, Z. Asadi, L. Zarei, S.B. Sadi, Z. Amirghofran, Spectrochim. Acta, Part A. 133 (2014) 697–706.

[32] M. Asadi, Z. Asadi, S.B. Sadi, L. Zarei, F.M. Baigi, Z. Amirghofran, Spectrochim. Acta, Part A. 122 (2014) 118–129.

[33] L.R. Falvello, S. Fernandez, R. Navarro, A. Rueda, E.P. Urriolabeitia, Inorg. Chem. 35 (1996) 3064-3066

[34] L.R. Falvello, S. Fernandez, R. Navarro, A. Rueda, E.P. Urriolabeitia, Organometallics. 17 (1998) 5887-5900.

[35] K. Karami, O. Buyukgungor, J. Coord. Chem. 62 (2009) 2949-2956.

[36] G. Gliemann, Ber. Bunsen-Ges. Phys. Chem. 82 (1978) 1263.

[37] K. Karami, O. Buyukgungor, H. Dalvand. Transition Met. Chem. 35 (2010) 621-626.

[38] K. Karami, C. Rizzoli, F. Borzooie, Polyhedron. 30 (2011) 778-784.

[39] S.J. Sabounchei, F.A. Bagherjeri, J. Lipkowski, M. Khalaj, J. Organomet. Chem. 696 (2011) 3521-3526.

[40] B.L. Fei, W. Li, W.S. Xu, Y.G. Li, J.Y. Long, Q.B. Liu, K.Z. Shao, Z.M. Su, W.Y. Sun, J. Photochem. Photobiol. B. 125 (2013) 32-41.

[41] H. Chao, W. Mei, Q. Huang, L. Ji, J. Inorg. Biochem. 92 (2002) 165-170.

[42] X.F. He, L. Wang, H. Chen, L. Xu, L.N. Ji, Polyhedron. 17 (1998) 3161-3166.

[43] A. Pyle, J. Rehmann, R. Meshoyrer, C. Kumar, N. Turro, J.K. Barton, J. Am. Chem. Soc. 111 (1989) 3051-3058.

[44] A. Wolfe, G.H. Shimer Jr, T. Meehan, Biochemistry. 26 (1987) 6392-6396.

[45] M. Anjomshoa, H. Hadadzadeh, S.J. Fatemi, M. Torkzadeh-Mahani, Spectrochim. Acta, Part A. 136 (2015) 205-215.

[46] N. Nanjundan, P. Selvakumar, R. Narayanasamy, R.A. Haque, K. Velmurugan, R. Nandhakumar, T. Silambarasan, R. Dhandapani, J. Photochem. Photobiol. B. 141 (2014) 176-185.

[47] L.Z. Zhang, G.Q. Tang, J. Photochem. Photobiol. B. 74 (2004) 119-125.

[48] M. Bordbar, M. Tabatabaee, M. Alizadeh-Nouqi, Z. Mehri-Lighvan, H.R. Khavasi, A. YeganehFaal, F. Fallahian, M. Dolati, J. Iran. Chem. Soc. 13 (2016) 1125-1132.

[49] I.S. Haworth, A.H. Elcock, J. Freemann, A. Rodger, W.G.J. Richards, J. Biomol. Struct. Dyn. 9 (1991) 23-44.

[50] M. Cory, D.D. McKee, J. Kagan, D.W. Henry, J.A. Miller, J. Am. Chem. Soc. 107 (1985) 2528-2536.

[51] T. Miyahara, H. Nakatsuji, H. Sugiyama, J. Phys. Chem. A. 117 (2012) 42–55.

[52] M. Bordbar, F. Khodaie, M. Tabatabaee, A. Yeganeh-Faal, Z.M. Lighvan, S. Mohammad-Ganji, Chem. Commun. 48 (2016) 422-429.

[53] X. Li, Y. Lin, Q. Wang, Y. Yuan, H. Zhang, X. Qian, Eur. J. Med. Chem. 46 (2011) 1274–1279.

[54] P.U. Maheswari, M. Palaniandavar, J. Inorg. Biochem. 98 (2004) 219–230.

[55] Z. Zhang, X.H. Qian, Int. J. Biol. Macromol. 38 (2006) 59‑64.

[56] K. Karami, Z.M. Lighvan, S.A. Barzani, A.Y. Faal, M. Poshteh-Shirani, T. Khayamian, V. Eigner, M. Dušek, New J. Chem. 39 (2015) 8708-8719.

[57] K. Karami, Z.M. Lighvan, A.M. Alizadeh, M. Poshteh-Shirani, T. Khayamian, J. Lipkowski, RSC. Adv. 6 (2016) 78424-78435.

[58] M. Chauhan, F. Arjmand, Chem. Biodivers. 3 (2006) 660-676.

[59] P. Kumar, S. Gorai, M.K. Santra, B. Mondal, D. Manna, Dalton Trans. 41 (2012) 7573-7581.

[60] G.J. Ryan, F.E. Poynton, R.B. Elmes, M. Erby, D.C. Williams, S.J. Quinn, T. Gunnlaugsson, Dalton Trans. 44 (2015) 16332-16344.

[61] Y. Geldmacher, R. Rubbiani, P. Wefelmeier, A. Prokop, I. Ott, W.S. Sheldrick, J. Organomet. Chem. 696 (2011) 1023-1031.

[62] S. Anbu, S. Kamalraj, B. Varghese, J. Muthumary, M. Kandaswamy, Inorg. Chem. 51 (2012) 5580-5592.

[63] B. Maity, M. Roy, S. Saha, A.R. Chakravarty, Organometallics. 28 (2009) 1495-1505.

[64] A. Sułkowska, J. Mol. Struct. 614 (2002) 227-232.

[65] M. Ganeshpandian, R. Loganathan, S. Ramakrishnan, A. Riyasdeen, M.A. Akbarsha, M. Palaniandavar, Polyhedron. 52 (2013) 924-938.

[66] M.R. Eftink, Top. Fluoresc. Spectrosc. (2002) 53-126.

[67] S. Lehrer, Biochemistry. 10 (1971) 3254-3263.

[68] A. Belatik, S. Hotchandani, J. Bariyanga, H. Tajmir ‐ Riahi, Eur. J. Inorg. Chem. 48 (2012) 114-123.

[69] T. Kosa, T. Maruyama, M. Otagiri, Pharm. Res. 14 (1997) 1607-1612.

[70] Q. Wang, X. Liu, M. Su, Z. Shi, H. Sun, New J. Chem. 38 (2014) 4092-4098.

[71] T. Ha, T. Enderle, D. Ogletree, D.S. Chemla, P.R. Selvin, S. Weiss, Proc. Natl. Acad. Sci (PNAS). 93 (1996) 6264-6268.

[72] D.E. Gomes, Í.P. Caruso, G.C. de Araujo, I.O. de Lourenço, F.A. de Melo, M.L. Cornélio, M.A. Fossey, F.P. de Souza, Int. J. Biol. Macromol. 85 (2016) 40-47.

[73] S.S. Maigali, M.A. Abd-El-Maksoud, F.M. Soliman, Arch. Pharm. 344 (2011) 442-450.

[74] J.D. Eckelbarger, J.T. Wilmot, M.T. Epperson, C.S. Thakur, D. Shum, C. Antczak, L. Tarassishin, H. Djaballah, D.Y. Gin, Chem. Eur. J. 14 (2008) 4293-4306.

[75] W. Zhang, Z. Zhang, Y. Zhang, Nanoscale Res Lett. 6 (2011) 555.

[76] N. Wang, L. Ye, F. Yan, R. Xu, J. Pharm. Sci. 351 (2008) 55-60.

[77] M. Gharagozlou, D.M. Boghaei, Spectrochim. Acta, A. 71 (2008) 1617-1622.

[78] F. Deng, Y. Liu, J. Lumin. 132 (2012) 443-448.

[79] Y. Song, Y. Liu, W. Liu, F.A. Villamena, J.L. Zweier, RSC Adv. 4 (2014) 47649-47656.

[80] Y.Y. Yue, X.G. Chen, J. Qin, X.J. Yao, J. Pharm. Biomed. Anal. 49 (2009) 753-759.

[81] Y.J. Hu, Y. Liu, L.X. Zhang, R.M. Zhao, S.S. Qu, J. Mol. Struct. 750 (2005) 174-178.

Figures captions

Scheme 1. (A) PPh_3, dichloromethane, 60 °C; (B) $Pd(OAc)_2$, methanol, room temperature, 24 h; (C) (PPh_3), (Py), dichloromethane, room temperature, 12 h.

Figure 1: ORTEP diagram of the complex **1**

Figure 2: UV-Vis of the complex 1 (A) and the complex 2 (B) in the buffer solution (5 mM Tris-HCl/50 mM NaCl at the pH of 7.2). Ahrough adding CT-DNA. [Complex] = 6×10^{-5} mol L^{-1}, [DNA] = 6×10^{-4}mol L^{-1}. The arrow shows that the absorption intensities reduces the enhanced DNA concentration. Supplement: Designs of [DNA]/[εa - εf] vs. [DNA] for the titration of the complexes with DNA.

Figure 3: Emission spectra of the DNA-MB set in the presence of the complex 1 (A) and the complex 2 (B). [DNA] = 6×10^{-5} M, [Complex] = $0–1 \times 10^{-5}$ M, [MB] = 6×10^{-6}M. The arrow demonstrates that the emission intensity is changed via increasing the complex concentration.

Figure 4: CD spectrum of [CT-DNA] = (1×10^{-4} mol L^{-1}) in the absence and presence of [complexes] = (6×10^{-5} mol L^{-1}) in the 5 Mm Tris HCl with the 50 Mm NaCl (pH 7.2).

Figure 5: Plots of the changes of absorbance at 250 nm of [CT-DNA] = (6×10^{-5} mol L^{-1}) on heating in the absence and presence of [complex] = (4×10^{-5} mol L^{-1}) in the 5 mM Tris HCl with the 50 Mm NaCl.

Figure 6: Emission spectra of BSA with the titration of the complex 1 (A) and the complex 2 (B). [BSA] = (6×10^{-6} M), [complex] = ($0–6 \times 10^{-5}$). The arrow displays the alteration by enhancing the amounts of the complex. Supplement: Plans of F_0/F vs [Q] $\times 10^6$.

Figure 7: The effect of site markers, Eosin-Y (site I), ibuprofen (site II) and digoxin (site III) upon the emission of the complex 1 (A) and the complex 2 (B), as connected to BSA. [BSA] = [site markers] = 6×10^{-6}M; [Complex] = ($0–6 \times 10^{-5}$ M). (- - - - free BSA).

Figure 8: The lowest binding free energy conformation of the complex **1** and BSA (A). The three-dimensional representation of the interaction between the complex **1** and the interacted residues. The green spheres present the hydrogen bond (B). Solid spheres indicate the close contacts and the yellow solid long lines represent π-cation and π–π stacking interactions (B and C), respectively. The two-dimesnional representation of the interactions between the

complex **1** and the residues prepared by LigPlot$^+$ v1.4.4 software. Hydrophobic interactions are indicated by the spoked arcs (D).

Figure 9: The lowest binding free energy conformation of the complex **2** and BSA (A). The three-dimesnional representation of the interaction between the complex **2** and the interacted residues. Solid spheres indicate the close contacts (B). The two-dimensional representation of the interactions between the complex **2** and the residues prepared by LigPlot$^+$ v1.4.4 software. Hydrophobic interactions, the hydrogen bond, and the external bond are indicated by the spoked arcs, the green dashed line and the purple line, respectively (C).

Figure 10: The lowest binding free energy conformation of the complex **1** and DNA. The groove binding mode of interaction is obvious (A). The three-dimensional representation of the interaction between the complex **1** and nucleotides. Solid spheres indicate the close contacts, the yellow solid long lines represent the π–π stacking interaction, and the green spheres present the hydrogen bonds (B and C). The two-dimesnional representation of the interactions between the complex 1 and nucleotides prepared by LigPlot$^+$ v1.4.4 software. Hydrophobic interactions are indicated by the spoked arcs (D).

Figure 11: The lowest binding free energy conformation of the complex **2** and DNA. The groove binding mode of interaction is obvious (A). The three-dimensional representation of the interaction between the complex 2 and nucleotides. Solid spheres indicate the close contacts (B). The two-dimensional representation of the interactions between the complex **2** and the nucleotides prepared by LigPlot$^+$ v1.4.4 software. Hydrophobic interactions, the hydrogen bond, and the external bond are indicated by the spoked arcs, the green dashed line and the purple line, respectively (C)**.**

Figure 5: Dose-dependent cytotoxic activity of Pd complexes versus K562 and Jurkat cancer cell lines (concentrations: -1, 1, 10, 25, 50 and 100 µM). Data are the average ± SD of three independent analyses. All information represent substantial differences from the untreated control by $p < 0.05$.

Figure 13: Effects of ylide ligand and Pd complexes on cell cycle phases of Jurkat and K562 cell lines. Cells were cultured in the presence of compounds at concentrations equal to IC_{50} values) for 48 h. After staining with propidium iodide changes in cell cycle phases were analyzed by flow cytometry. Cells treated only with DMSO solvent at the highest concentration used in the tests were considered as negative control (C-). Data were statistically analyzed by one-way analysis of variance and presented as mean ± standard error of three independent experiments. **p<0.01, ***p<0.001 are for the percentage of cells accumulated in subG1 phase compared to the negative control.

Figure 14: Flow cytometry analysis of the effects of ylide ligand and Pd complexes on cell cycle phases of Jurkat and K562 cell lines. Histograms are representative of one experiment out of three independent experiments.

Figure 6: The overlap region between BSA fluorescence and the complex 1, 2 spectrum. [BSA] = [Complex] =10µM.

Table 1: Selected bond lengths (Å) and angles (°)

Table 2: The calculated amounts of K_b (M^{-1}) for the free complexes and the competition of the site marker via testing the complex –BSA system

Table 3: The measured distance between the complex 1 with BSA and DNA residues. The three-dimensional interaction mode of these non-covalent interactions in this table is indicated in the related figures.

Table 4: Cytotoxicity data (IC50) of the ylide ligand and palladium (II) complexes against K562 and Jurkat cancer cell lines

Scheme 1

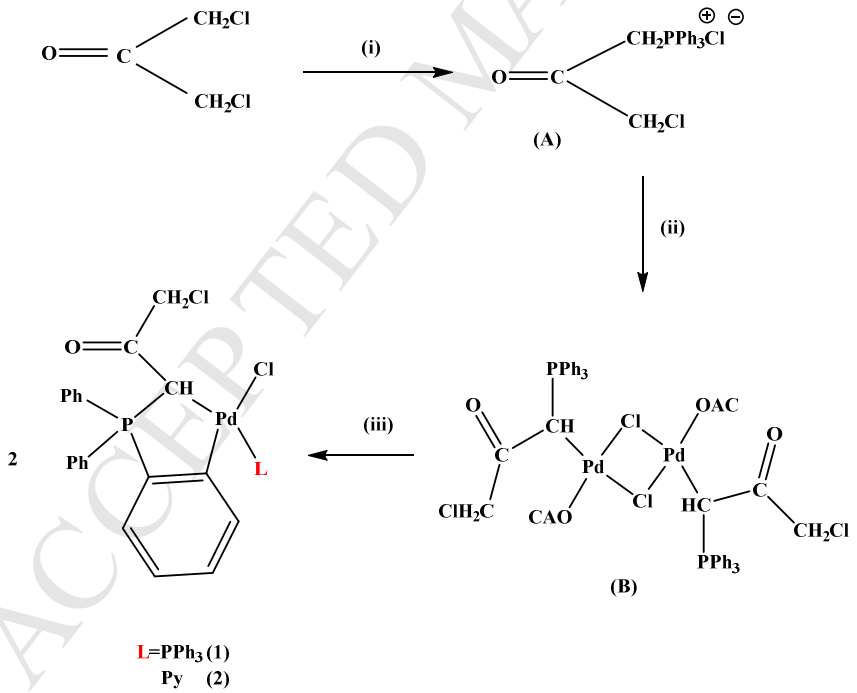

Figure 1

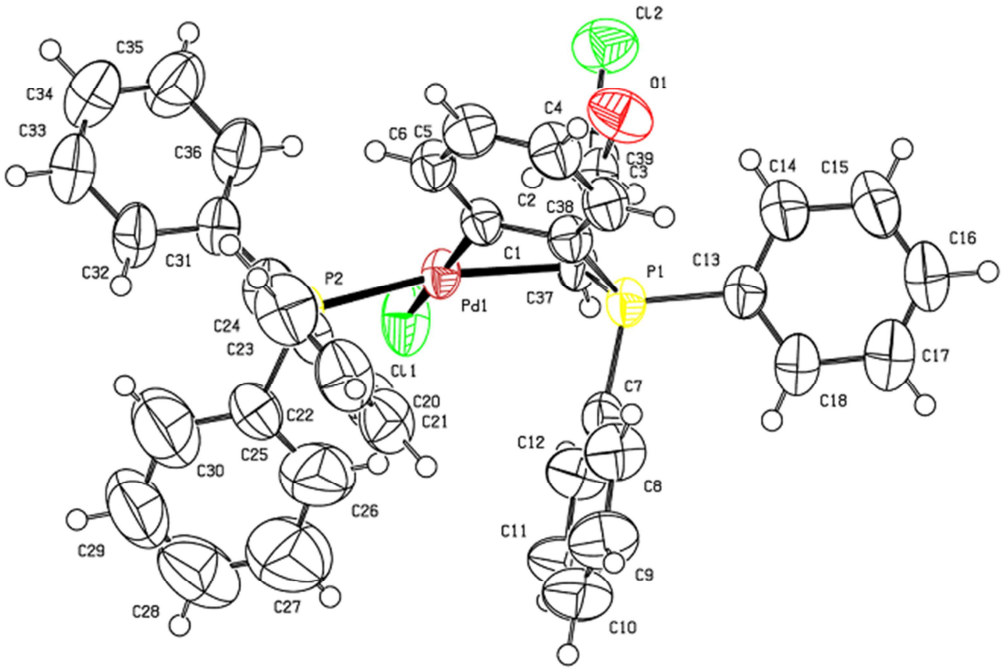

Figure 2

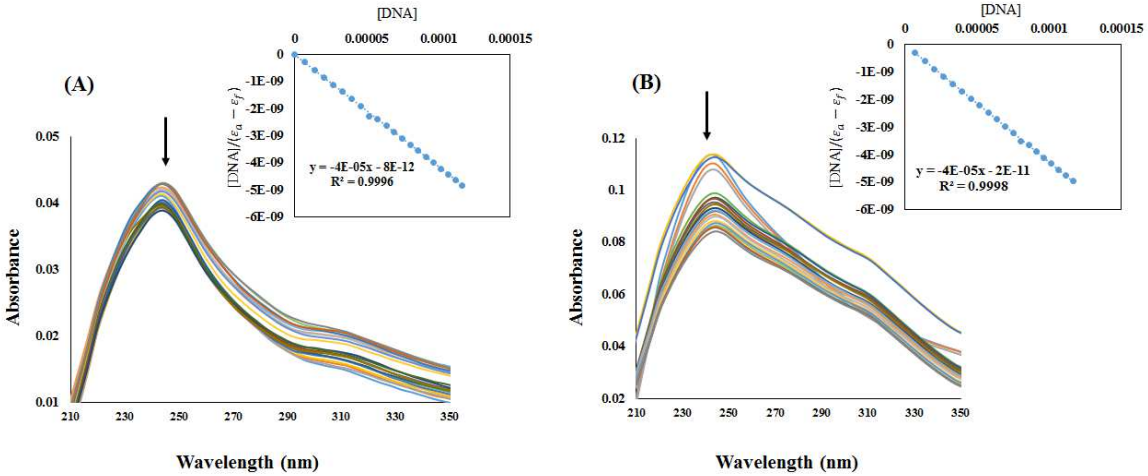

Figure 3

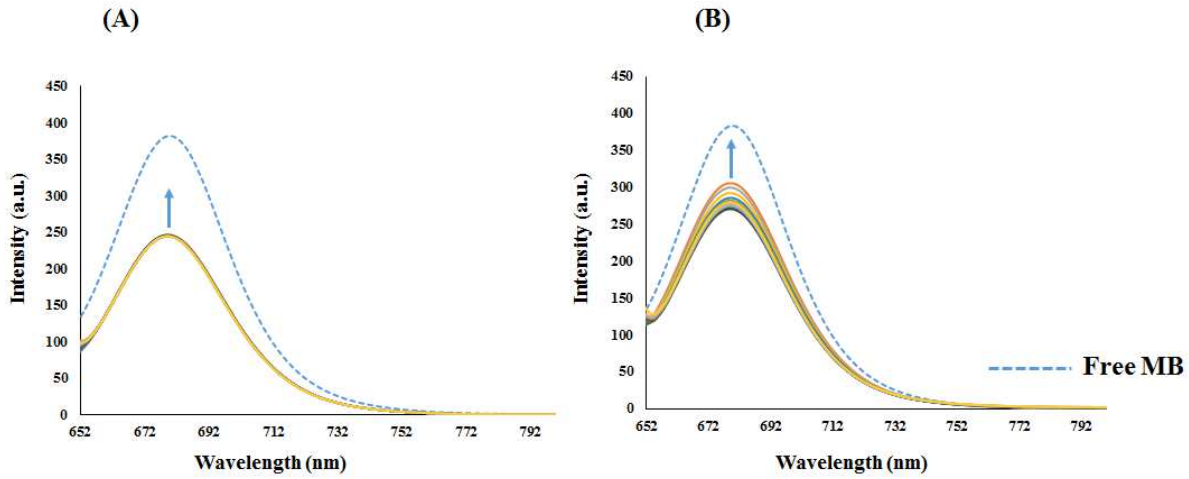

Figure 4

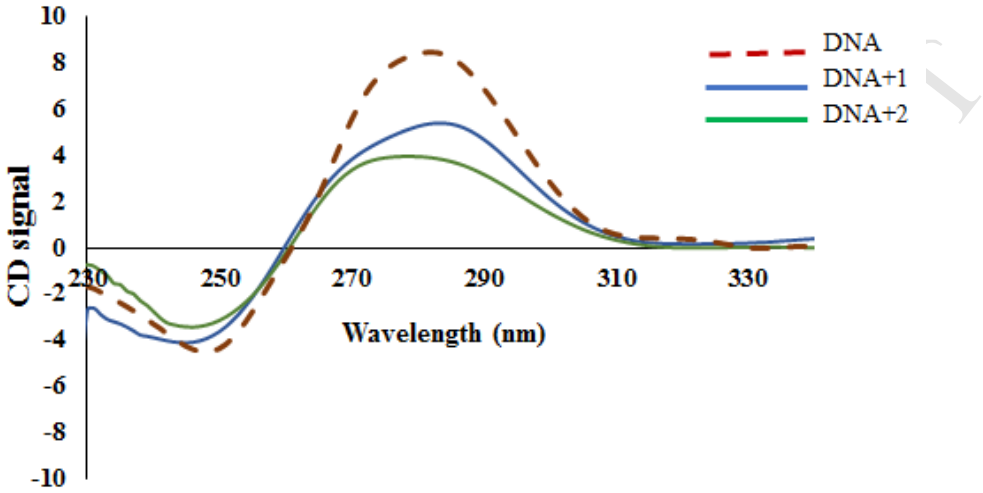

Figure 5

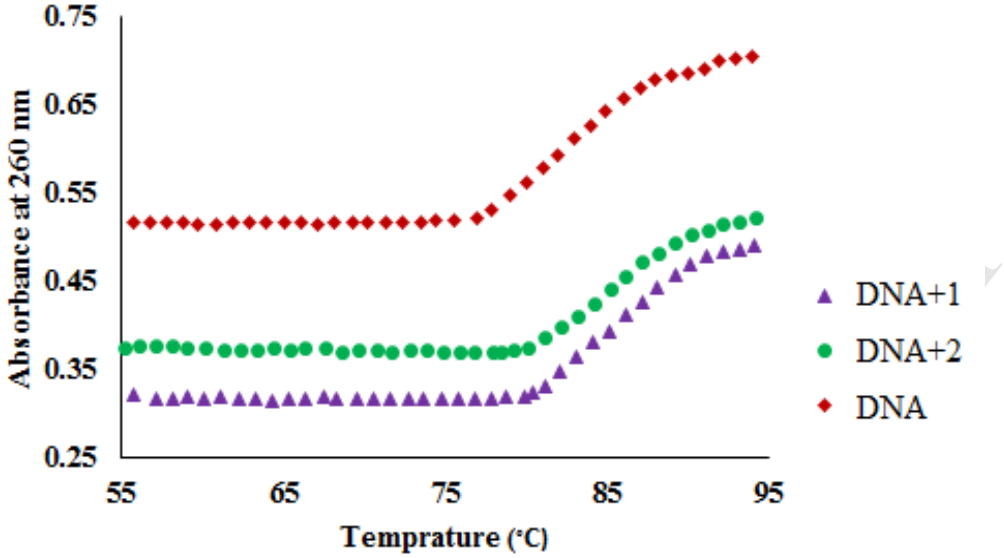

Figure 6

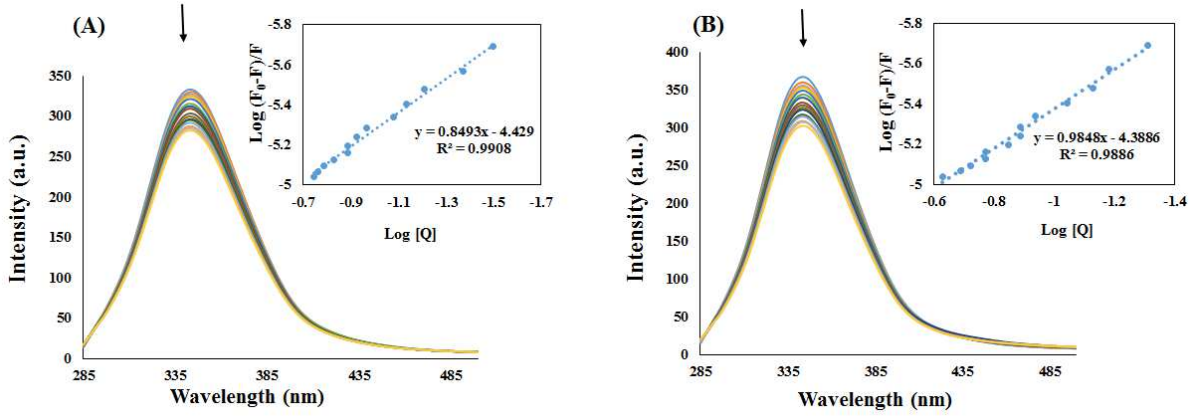

Figure 7

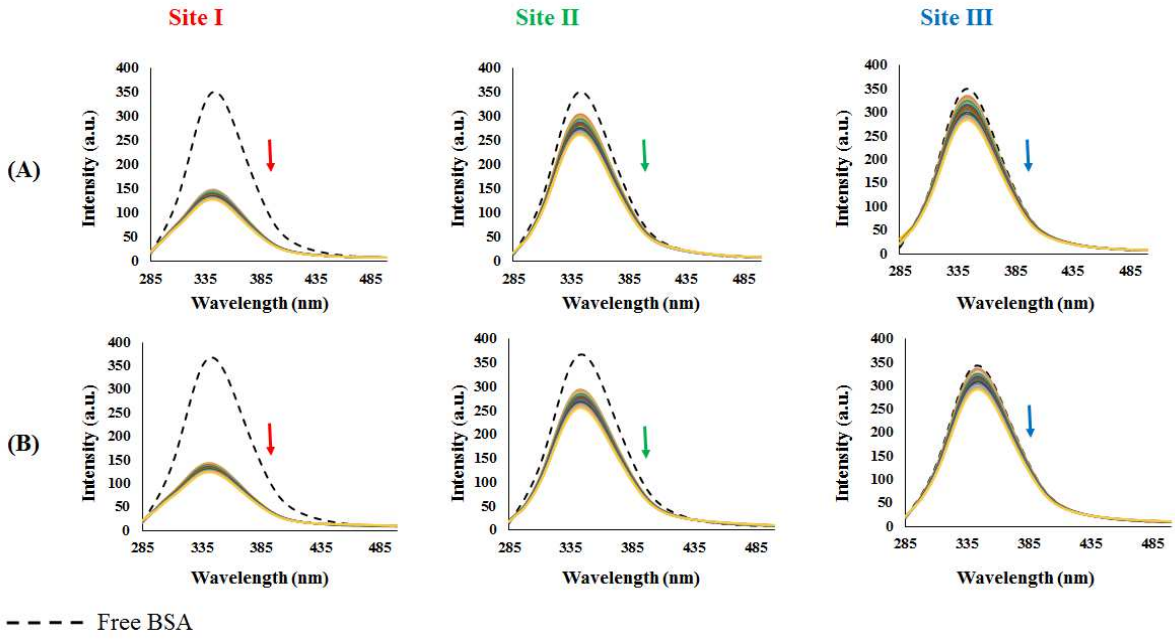

Figure 8

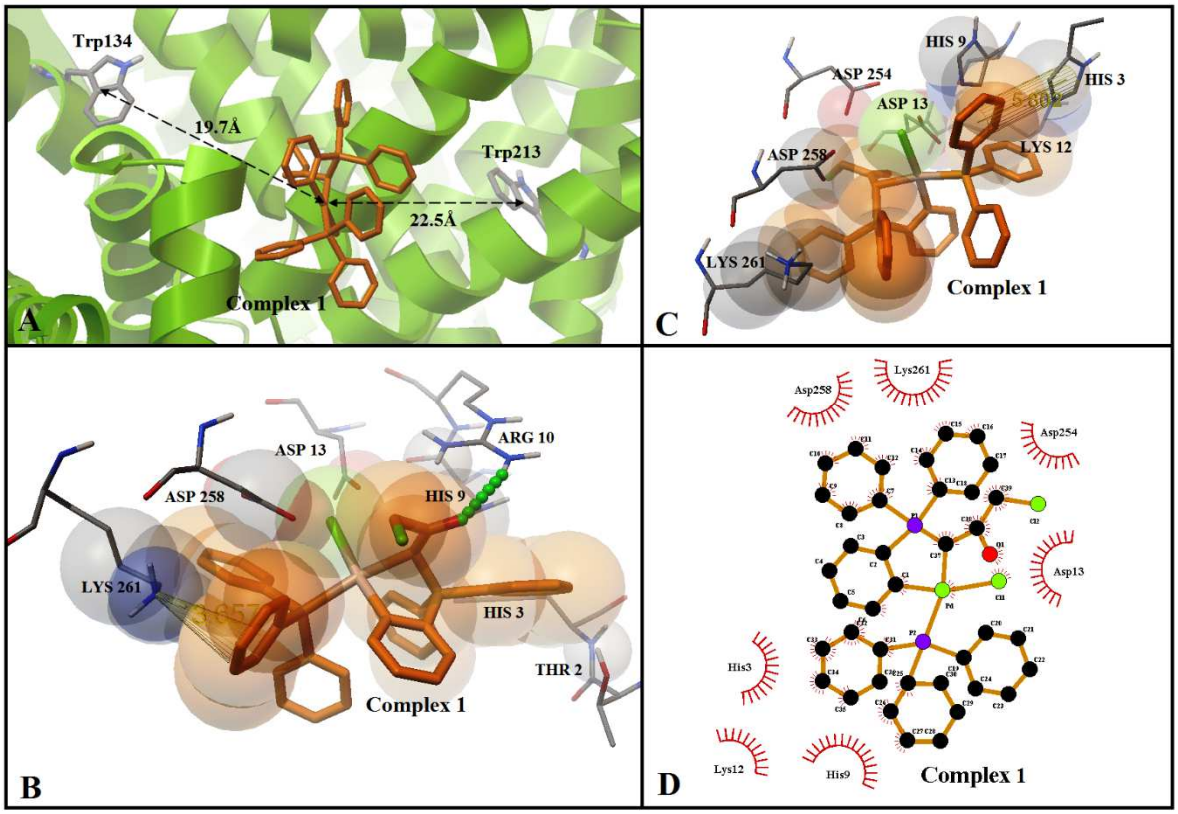

Figure 9

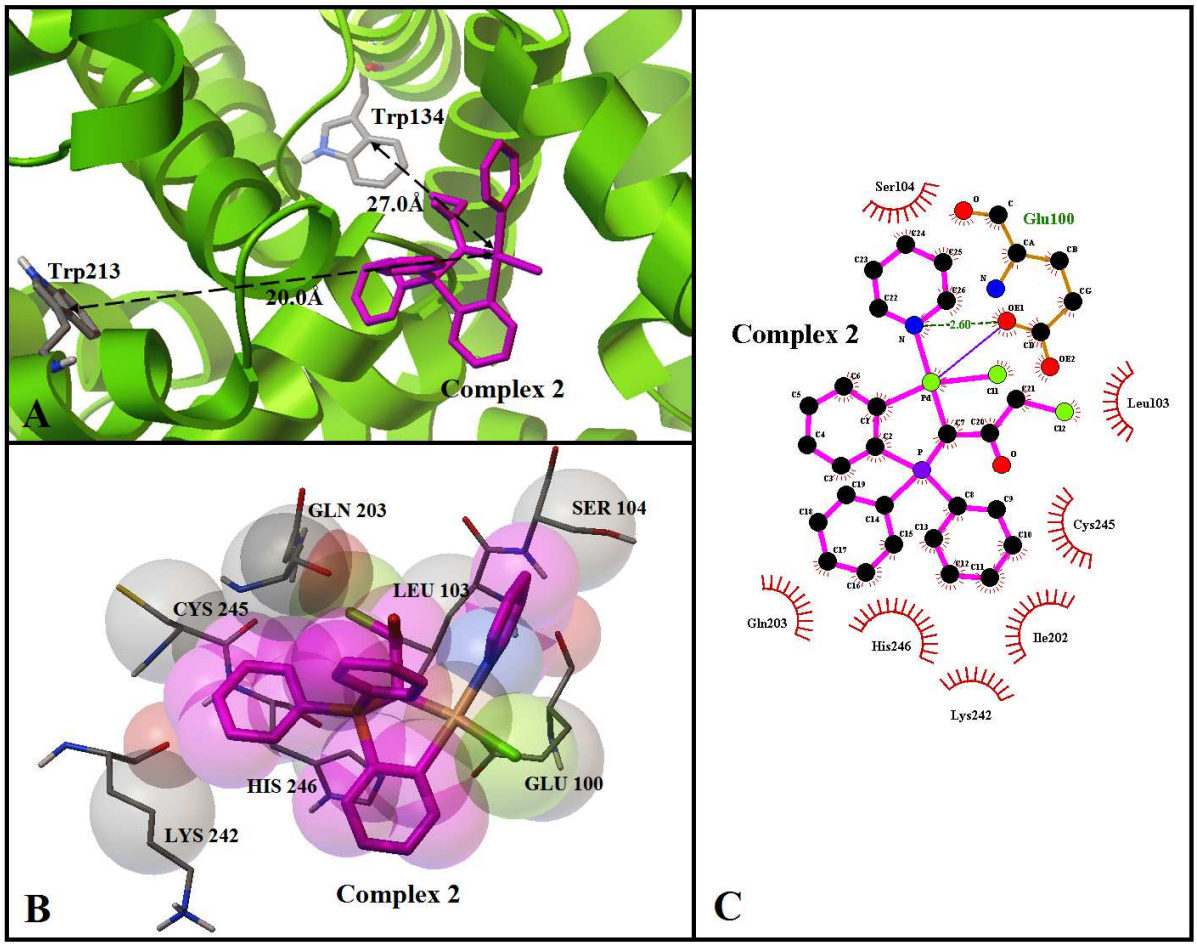

Figure 10

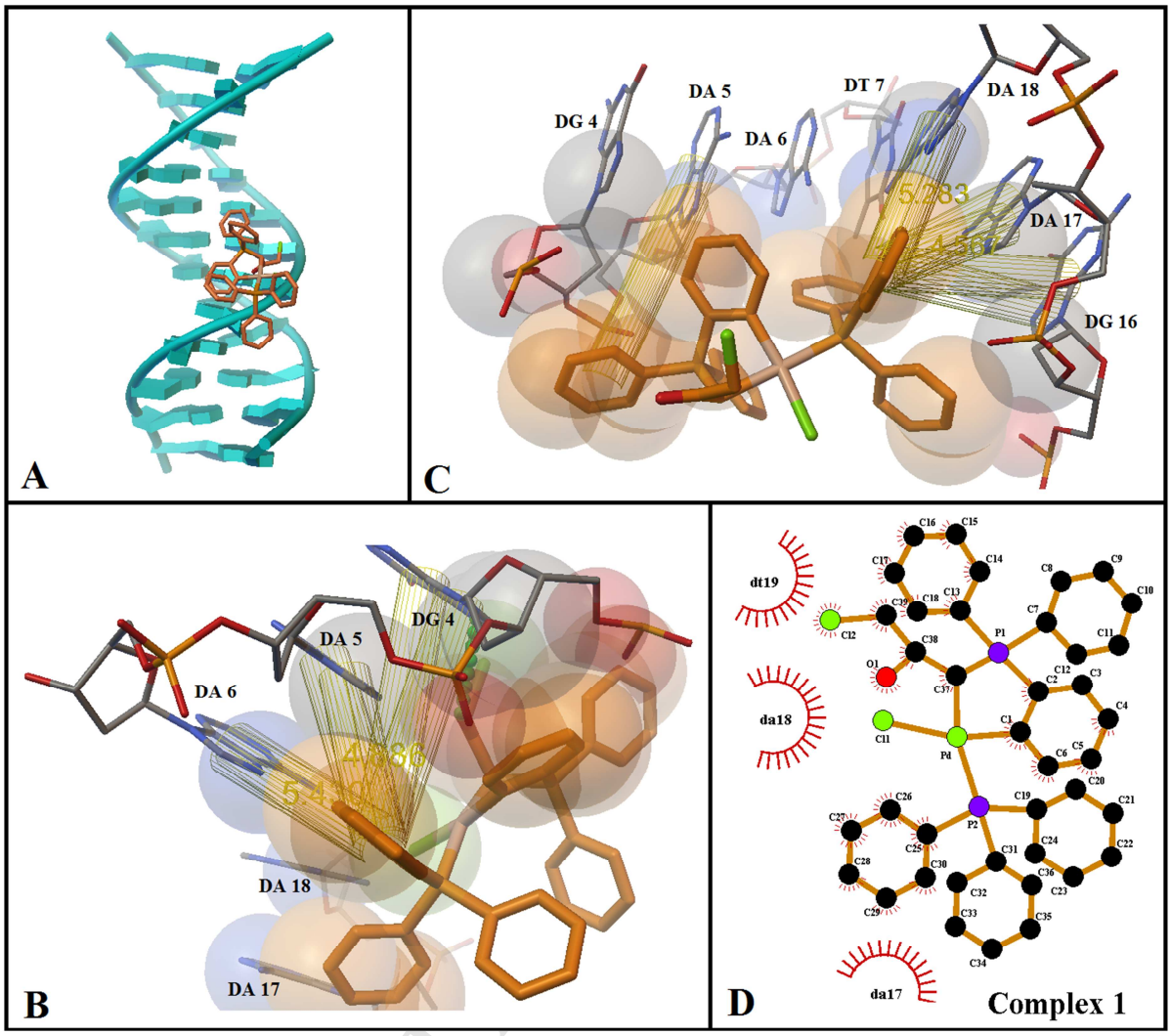

Figure 11

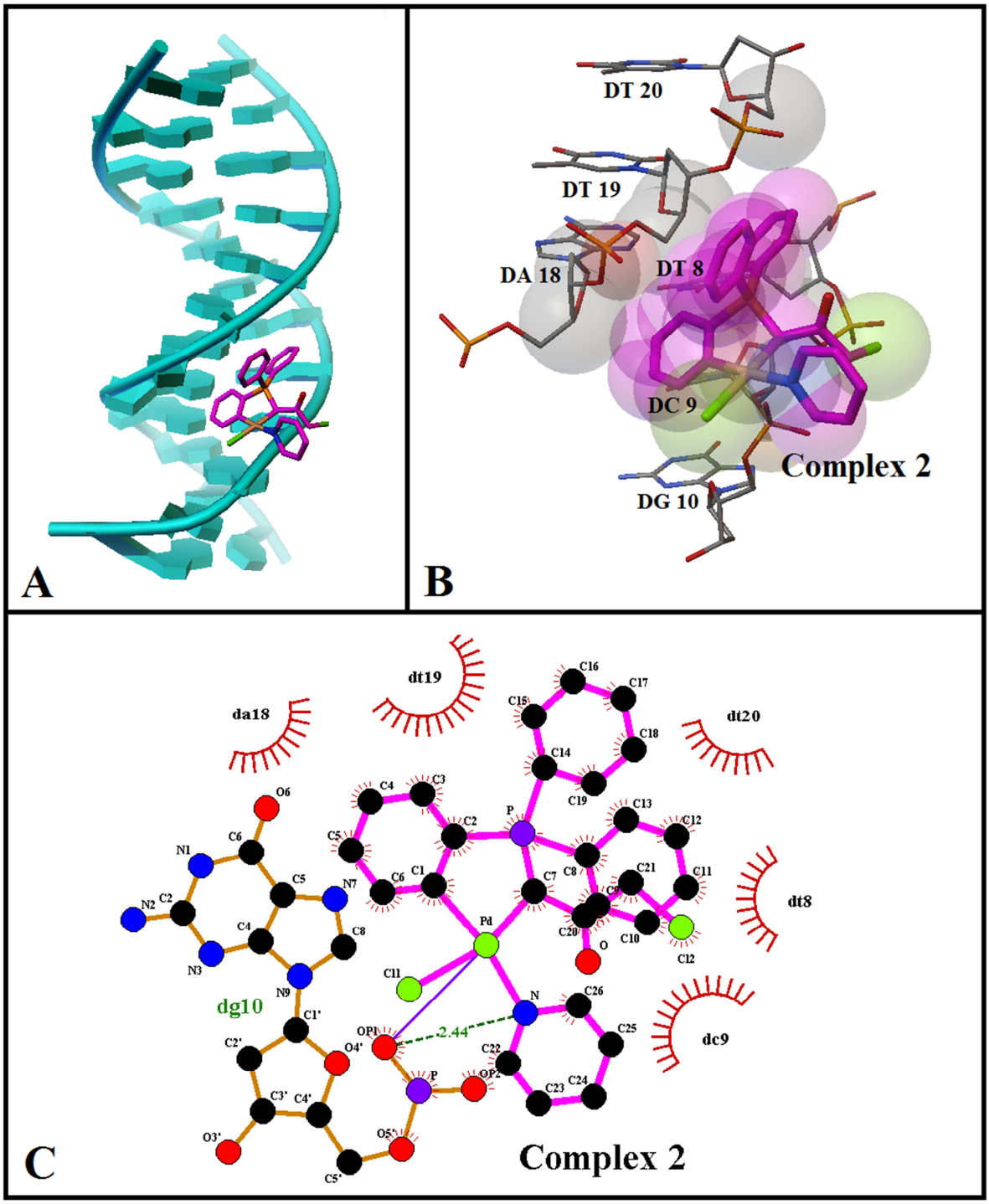
A
B
DT 20
DT 19
DA 18
DT 8
DC 9
DG 10
Complex 2
C
dt19
da18
dt20
dt8
dc9
dg10
2.44
Complex 2

Figure 12

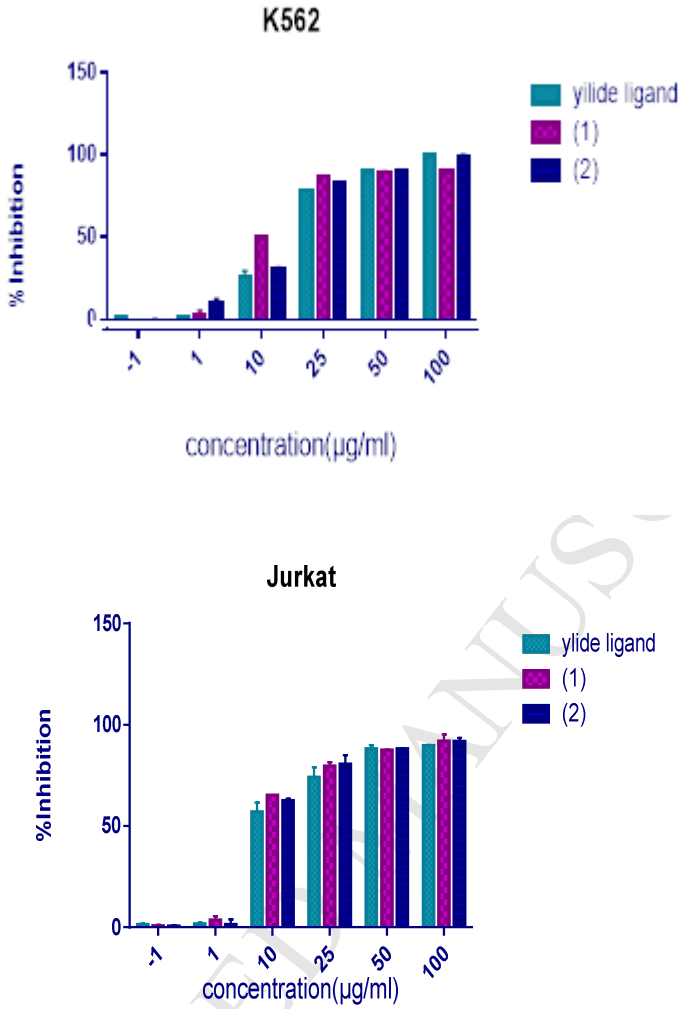

Figure 13

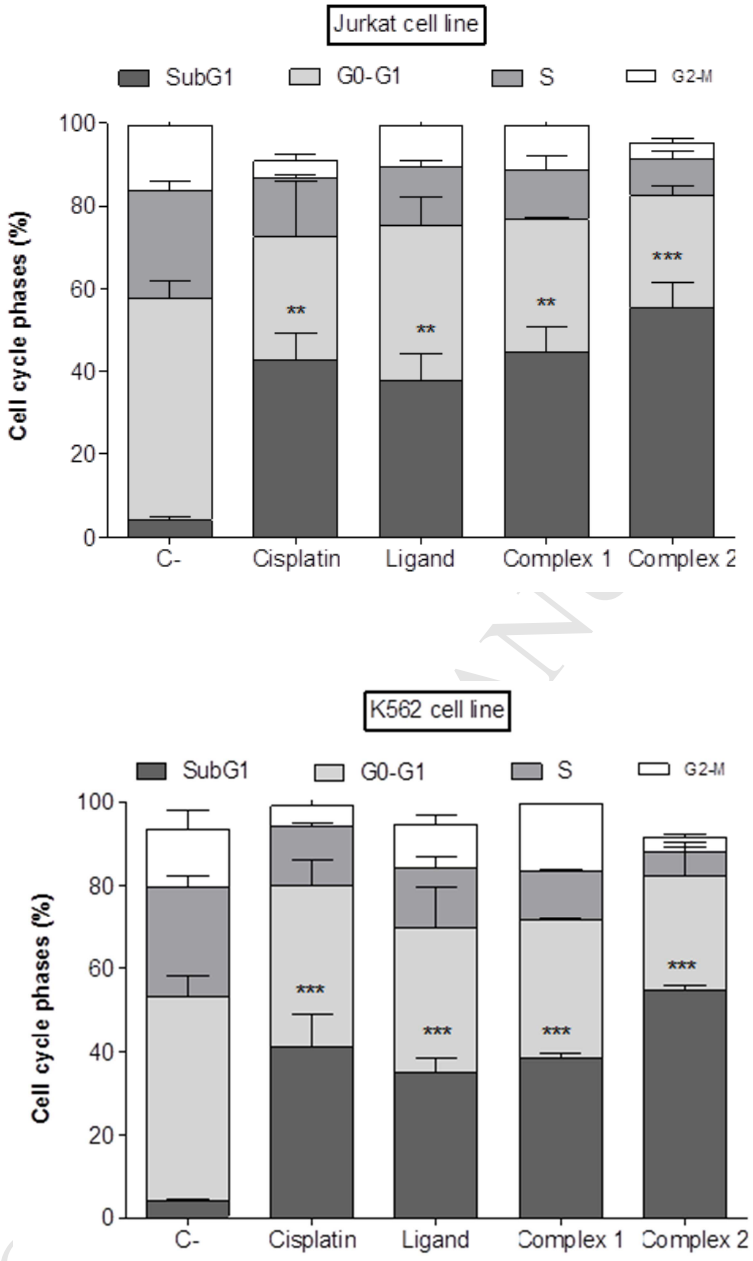
Jurkat cell line
SubG1
G0-G1
S
G2-M
Cell cycle phases (%)
100
80
60
40
20
0
**
**
**
***
C-
Cisplatin
Ligand
Complex 1
Complex 2
K562 cell line
SubG1
G0-G1
S
G2-M
Cell cycle phases (%)
100
80
60
40
20
0
***
***
***
***
C-
Cisplatin
Ligand
Complex 1
Complex 2

Figure 14

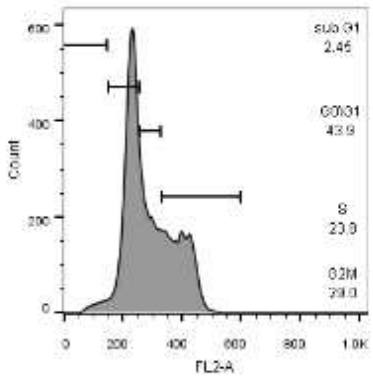

Negative control (Jurkat)

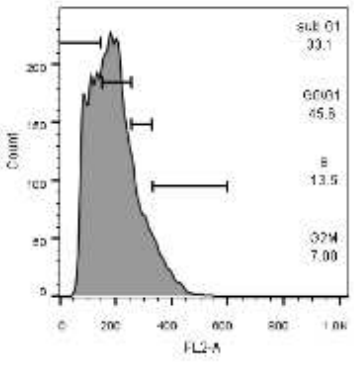

Cisplatin (Jurkat)

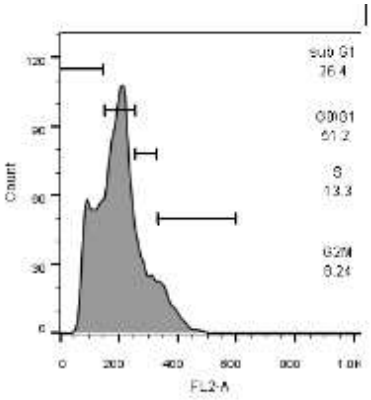

Ligand (Jurkat)

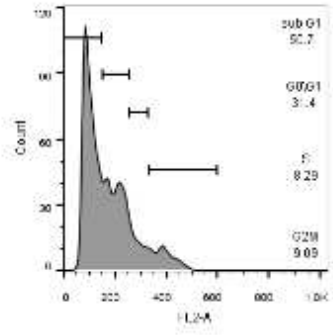

Complex 1 (Jurkat)

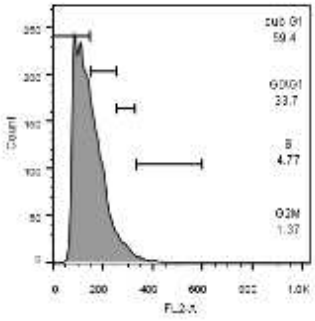

Complex 2 (Jurkat)

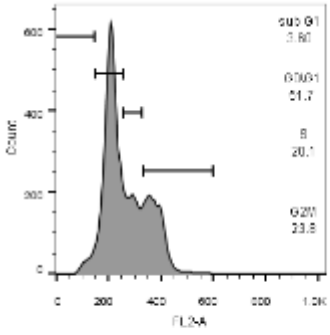

Negative control (K562)

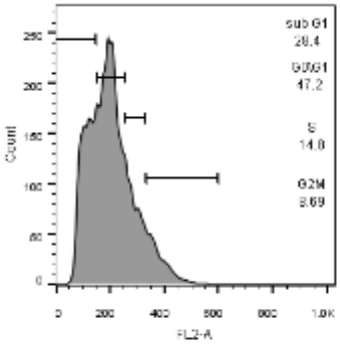

Cisplatin (K562)

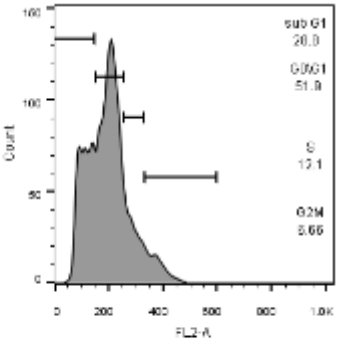

Ligand (K562)

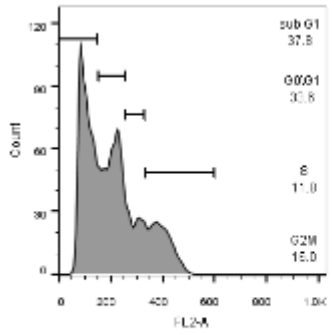

Complex 1 (K562)

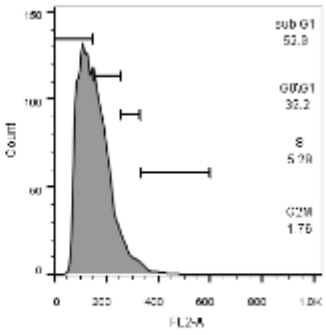

Complex 2 (K562)

Figure 7

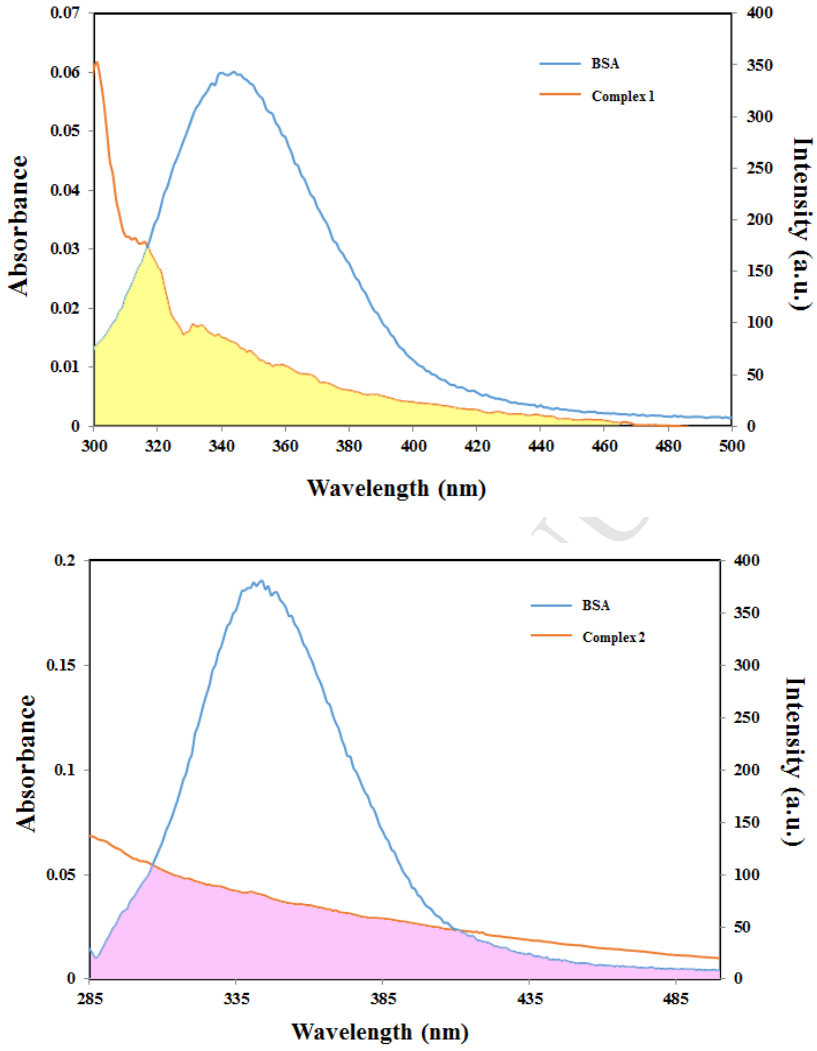
Absorbance
Intensity (a.u.)
Wavelength (nm)
BSA
Complex 1
0.07
0.06
0.05
0.04
0.03
0.02
0.01
0
400
350
300
250
200
150
100
50
0
300
320
340
360
380
400
420
440
460
480
500
Absorbance
Intensity (a.u.)
Wavelength (nm)
BSA
Complex 2
0.2
0.15
0.1
0.05
0
400
350
300
250
200
150
100
50
0
285
335
385
435
485

Table 1

Atoms	*Bond lengths*	*Atoms*	*Bond angles*
C1—Pd1	2.001 (4)	C1—Pd1—C37	85.44 (16)
C37—Pd1	2.144 (4)	C1—Pd1—P2	92.40 (12)
Cl1—Pd1	2.3828 (12)	C37—Pd1—P2	167.50 (14)
P2—Pd1	2.3108 (12)	C1—Pd1—Cl1	171.31 (14)
C25—P2	1.834 (4)	C37—Pd1—Cl1	88.41 (12)
C31—P2	1.821 (5)	P2—Pd1—Cl1	94.91 (5)
C19—P2	1.823 (5)		

Table 2

	BSA	BSA-Eosin-Y	BSA-ibuprofen	BSA-digoxin
Complex 1	1.59×10^{6}	6.2×10^{4}	1.56×10^{6}	1.37×10^{6}
Complex 2	1.74×10^{6}	1.37×10^{6}	1.73×10^{5}	1.21×10^{6}

Table 3

Bio-macromolecule	Interacting residue	Non-covalent Bonding/Interactions	Distance
BSA	Complex 1:UNK1:O1-BSA:Arg10:HH	Hydrogen Bonding	2.1Å
BSA	Complex 1:UNK1- BSA:Lys261:NZ	π-cation interactions	3.6Å
BSA	Complex 1:UNK1-BSA:His3	π–π stacking interactions	5.8Å
DNA	Complex 1:UNK1:O1-DNA:DG4:N7	Hydrogen Bonding	2.8 Å
DNA	Complex 1:UNK1-DNA:DA5	π–π stacking interactions	4.8 Å
DNA	Complex 1:UNK1- DNA:DA6	π–π stacking interactions	5.4 Å
DNA	Complex 1:UNK1- DNA:DA17	π–π stacking interactions	4.5 Å
DNA	Complex 1:UNK1- DNA:DA18	π–π stacking interactions	5.2 Å

Table 4

	K562	**Jurkat**
Ligand	18.5±1	8.5±0.5
Complex 1	11.2±1	7.5±0.6
Complex 2	15.6±1	7.7±0.4
Cisplatin	19.4±0.9	25±1.2

- The reactivity and coordination chemistry of phosphorous ylides are important.
- The complex was characterized by single crystal X-ray diffraction study.
- The complexes interact with CT-DNA via groove binding with partial intercalation.
- The complexes exhibit significant in vitro cytotoxicity against cancer cell lines.